nature portfolio

Peer Review File

Customized composition of lithium metal solid-electrolyte interphase by electric field modulation of anion motion direction

Corresponding Author: Professor Jun Lu

This file contains all reviewer reports in order by version, followed by all author rebuttals in order by version.

Version 0:

Reviewer comments:

Reviewer #1

(Remarks to the Author)
This manuscript presents an electrolyte formulation by mixing three different lithium salts with a flame-retardant solvent. The authors claim that the proposed electrolyte exhibits superior electrochemical properties compared to a conventional 1 M $LiPF_6$/EC-DMC electrolyte, attributing this enhancement to the cooperative effect of the three anions in forming a robust protective layer on the electrode surface. However, the manuscript contains numerous deficiencies, with significant shortcomings in the analysis used to support its conclusions. Consequently, the reviewer finds that this work does not meet the high standards of Nature Communications. The key issues are as follows:

1. The manuscript adopts 1 M $LiPF_6$/EC-DMC as the benchmark electrolyte. However, it is well known that this electrolyte undergoes severe degradation when paired with a lithium metal anode. This choice appears to be a deliberate attempt to exaggerate the performance of the proposed electrolyte. To substantiate the claim of superior performance, a comparison should be made against state-of-the-art imide-based electrolytes.

2. The study employs molecular dynamics simulations of the Li electrode–electrolyte interface under an applied electric field, yet several methodological issues undermine the reliability of these calculations. First, the interaction between lithium metal and the electrolyte cannot be accurately described using a standard classical force field (OPLS-AA), as it severely underestimates adsorption strength compared to first-principles calculations. Additionally, an excessively high electric field (-1.0 V/nm) is applied to the electrode surface, leading to an unrealistic accumulation of Li ions at the interface, which likely affects the anion distribution as well. Since the proposed mechanistic interpretation relies solely on simulation results, further efforts are required to ensure an accurate representation of ion distributions at the Li metal surface.

3. The proposed mechanism is based on differences in ion distributions within a sub-nanometer scale. However, the spatial scale of the solid electrolyte interphase (SEI) typically ranges from 10 to 100 nm. Thus, the claim that such minor initial variations directly translate into the experimentally observed SEI composition lacks sufficient justification.

4. $LiNO_3$ is widely recognized as an additive that stabilizes the SEI layer, improving both film stability and battery lifespan. The inclusion of $LiNO_3$ in the electrolyte and its reported effects do not present a novel finding.

5. If the cooperative effect of three anions is to be claimed as a central finding, it is necessary to consider a broader range of anionic species to evaluate the generality of the proposed mechanism. Without such validation, the novelty of the proposed strategy remains questionable.

Reviewer #2

(Remarks to the Author)
1. The article is interesting, and reveals a layered SEI formed by ternary lithium salts: an inner layer composed of Li3N and B-O, and an outer layer of LiF, achieving a comprehensive performance of high ionic conductivity, mechanical strength, and toughness for the SEI. The results in the manuscript are very meaningful for the development of lithium metal batteries, and I

would like to try a industrial demo according to the reported cell design after the manuscript, of course, will be published.
2. According to the results of the radial distribution function, regardless of whether an electric field is applied, TEP still predominates on the lithium metal surface. Following the authors' design logic, higher lithium salt concentrations may result in better SEI formation efficiency. The understanding of the optimized 0.5M-DBN should be addressed.
3. In line 165, "electrical conductivity" is suggested to be more accurately changed to "ionic conductivity".
4. The experiment uses the electrolyte of LiPF6/carbonate as the reference, while the electrolyte of TEP/three salts is a completely different recipe. It would be more convincing if a comparison of carbonate/three salts with LiPF6/carbonate will be adopted.
5. It is unclear that the first appearance of 1.5 M-N in line 171 while its explanation is in line 213. This should be revised for clarity.
6. Are the three salt concentrations in 0.5-DBN all 0.5 mol? The 1.5M-N electrolyte is noted later as 1.5 mmol, which makes the comparison of SEI strength in line 171 meaningless.
7. In line 212, is the salt concentration also in mmol? Comparing to the total salt concentration of 1.5 mol in 0.5M-DBN, it is also not appropriate.
8. Figure S1b shows that the ionic conductivity of 0.4 M-DBM is 4.92 mS/cm, but in Figure S1c, the ionic conductivity of 0.4 M-DBM is shown as 3.86 mS/cm. Please confirm the actual ionic conductivity of the electrolyte.
9. In Figure 2a, there is a typo in "In-suit Fourier-transform Infrared (FTIR) spectra". The spectra provided in the article are difficult to be interpreted in terms of the trends of the signal peaks. It would be more helpful to present the data as Contour plots.
10. The initial discharge capacity of 2.8-4.5 V (Figure 5b & Figure S39) at 0.5 C is lower than that of 2.8-4.3 V (Figure 5a) at 1 C. How to understand?
11. In Figure 5l "DLi+ of NCM523 cathode" should be "DLi+ of NCM811 cathode"?
12. The author claims that the GED of the pouch cell is 452.47 Wh/kg, the battery design in detail needs to be clarified.
13. TEP based electrolyte could be retardant at a content of 5-10% wt. The molecule itself has a high reactivity with lithium metal, which has been reflected in the optimized coulombic efficiency of only 97.5%. This coulombic efficiency makes it difficult for practical applications in lithium metal cells. Does the author compare TEP to other retardant solvents?
14. Fig "S33" in line 327 should actually be Fig S37. Please confirm.

Reviewer #3

(Remarks to the Author)
This manuscript reports a non-flammable phosphate-based electrolyte for lithium metal batteries using a ternary-salt combination of LiDFOB, LiNO3, and LiBF4 in triethyl phosphate (TEP). The electrolyte facilitates the formation of a solid electrolyte interphase (SEI) enriched with B-O and Li3N in the inner layer and LiF in the outer layer, contributing to improved stability and reversibility of the lithium metal anode. While the study presents comprehensive characterization, its novelty does not appear to lie in new material design or good performance. A similar electrolyte formulation of 1 M LiDFOB together with 0.2 M LiNO3 dissolved in TEP, ethylene carbonate (EC) and dimethyl carbonate (DMC), with better Li metal stability (Coulombic efficiency of ~98% vs. 97.2% in this work), has been reported several years ago in the Journal of Electrochemical Society (J. Electrochem. Soc., 166, A2523). Moreover, some other phosphate electrolytes in literatures have also shown comparable and higher CE with non-flammable feature (e.g., Batteries & Supercaps, 2023, 6, e202200453; Batteries & Supercaps, 5, e202100407; Energy Storage Materials, 2024, 71, 103603; ACS Nano 2023, 17, 23, 24227–24241). However, this work may potentially provide some insights in the mechanistic understanding, if some unclear points can be clarified.

Major comments:
1. The key finding of this work is the contrasting response of DFOB-/NO3- anions vs. BF- anion under electric field, where the former migrate towards Li metal anode while the latter move away, as evidenced by molecular dynamic (MD) simulations. This phenomenon is thought to drive the preferential reduction of DFOB- and NO3- anions to form an SEI with B-O and Li3N-rich inner layer and LiF-rich outer layer.

If this phenomenon truly occurs in lithium metal batteries, it would be interesting. However, there are several unclear points. The first is concerning the model of MD calculations. Does it consider the effect of electric double layer in the calculation? If not, the electric double layer itself has a species distribution, which might violate the calculation results in the paper, i.e., DFOB-, NO3- and BF4- anions do not move in behaviors predicted by the MD simulation results. Second, since the Li+ ion is coordinated with DFOB-, NO3- or BF4- anion to form the charge-neutral ion pair, why can the anions in the ion pair move towards the Li metal anode under electric field? Third, what's the meaning of y axis in Figure 1c-1f? Does it reflect the real content of anions and solvents close to Li(100)? If it is, then why all anions and solvents just sum up to ~10%? Fourth, what's the rational of choosing Li(100) for calculation rather than Li(110), the thermodynamically most stable plane, or other Li planes? The fifth point, the statistcal distribution of DFOB-, NO3- and BF4- does not differ too much in Figure 1c-1f, ~1.0 for the former peak and 0.8 for the BF4- peak. It is not a significant difference for the amount of DFOB-, NO3- and BF4- on Li surface.

2. For the in-situ FTIR test which can potentially validate the MD simulation results, there are also many confusing issues. The manuscript writes that "during plating, …Notably, the reversibility of BF_4^- is significantly higher compared to that of $ODFB^-$, indicating that $ODFB^-$ is more extensively consumed". This phenomenon is difficult to interpret, since the electrode polarization should be negative for the plating process in Li/Cu cell, which will expel the negatively charged anions from Li metal surface instead of increasing their concentration. On the other point of view, the decrease in DFPB- intensity might be attributed to the negative electric field rather than the consumption of DFPB-.
A more fatal defect of the FTIR result is the strong intensity of BF4- on the Li surface, which is completely contradictory to the

MD results in Figure 1 which claims that BF4- can hardly approach the Li metal and thus weakens its reduction. The discrepancy between the FTIR observation and the MD simulation highlights a significant gap in the study's coherence. Also, the LiF and free TEP peaks are almost not visible, whose change cannot be discerned during test. This is problematic because these peaks are expected to be critical indicators of the formation and evolution of the SEI, and their absence raises doubts about the accuracy of the in-situ FTIR analysis or the interpretation of the spectra.

3. The formation mechanism of dual-layered SEI is not clear.
Since DFOB- can be decomposed to form B-O species in the inner SEI, why can't we detect large amount of LiF in the inner layer, given that DFOB- can donate element F during decomposition?

4. What's the role BF4- plays in this electrolyte? From the paper, it seems that the binary combination of DFOB- and NO3- can have a positive effect on the Li metal anode.

5. The reported Coulombic efficiency values of Li/Li symmetic cells are very confusing and potentially misleading. The manuscript states that "the Li||Li symmetric battery assembled with 0.5 M-DBN electrolyte demonstrated a higher CE of 99.18% after 10 cycles at a current density of 0.25 mA cm-2 and with an area capacity of 0.5 mAh cm-2 than the Li||lithium symmetric batteries assembled with 0.75 M-DB (94.53%), 1.5 M-N (87.89%), and 1M LiPF6 EC/DMC (88.34%) electrolytes". However, since Li reserivor is super excesive in the Li/Li cell, how can the authors calculate the CE? This expression may not be considered professional or appropriate in a Li metal battery study.

6. The cathode degradation comparsion with XRD characterizations (Figure 4c-4e) does not perform in the perfectly same condition for the reported electrolyte and base electrolyte. The LiPF6 EC/DMC electrolyte has a higher ionic conductivity, thus enabling higher initial discharge capacity for Li/NMC811 cell. This corresponds to higher utilization rate of Li in the NMC811 cathode under the same cut-off voltage. Since it is widely accepted that the degradation of high-Ni cathode is closely linked to the Li de-intecalation ratio, the higher Li de-intecalation for cathode in the base LiPF6 EC/DMC electrolyte can leads to faster cathode degradation.
Considering that XRD peak shift is comparable for both the reported electrolyte and base electrolyte, it is unclear that the cathode degradation is caused by the electrolyte itself or merely due to the different Li deintecalation ratio.

7. The signal of LixC on the NMC811 cathode side is interesting. How can such a highly reducing material exist in the high voltage environment?

8. The calculation method of energy density of pouch cell is vague. Does it contain the weight of Al package? It is challenging to obtain such a high energy density with a relative high E/C ratio of 1.75 g/Ah. If the Al package weight was excluded, what's the real energy density for the cell?

Minor comments

1. Some other confusing points. For instance, "the height of layer deposited at the anode side is greater and the clump-like dendritic are larger when using the 0.5 M-DBN electrolyte than that of battery with 1 M LiPF6 EC/DMC electrolyte." This means that the Li metal is more porous in the reported electrolyte, which is not favorable.

"the leakage current density observed with the 1 M LiPF6 EC/DMC electrolyte (10.17 mA cm-2)". mA level leakage current is so large, which can be larger than the current for cell test.

2. "relatively complete and uniform CEI can … prevent unexpected electron transfer on the cathode/electrolyte interface". First, what's a complete SEI and unexpected electron transfer? Second, why a complete CEI can prevent unexpected electron transfer?

3. Some typo and grammar errors, e.g., "Successful decreasing the possibility of the parasitic reaction"

Version 1:

Reviewer comments:

Reviewer #1

(Remarks to the Author)
While the authors have addressed some initial concerns, critical issues remain unresolved, particularly regarding the mechanistic interpretation and its theoretical foundation. Without substantial revisions, the manuscript is not suitable for publication.

1. The use of the OPLS-AA force field for lithium metal, combined with a strong electric field of -1.0 V/nm, remains problematic. Although the authors cite precedent, they do not demonstrate that the observed ion migration trends persist under more realistic conditions. As the force field does not capture specific adsorption at the Li surface, the model likely exaggerates interfacial differences under the applied field. More seriously, despite the strong electric field, the anion distributions are noisy, and the field-induced effects cannot be clearly distinguished, raising serious concerns about the validity of the proposed mechanism. Furthermore, the SEI depth profiles, which the authors emphasize as key experimental evidence, reflect cumulative decomposition and transport processes over extended cycling and therefore do not directly

validate the simulated initial anion distributions.

2. The proposed link between the initial anion distribution and the long-term SEI layering remains speculative. Continued LiODFB consumption does not ensure sustained interfacial enrichment. Over extended cycling, differences in anion transport properties are likely to dominate, and without direct evidence, the proposed mechanism is not convincingly supported.

3. The two additional binary systems (LiDOB + LiFSI and LiNO3 + LiTFSI) provide some insight but are insufficient to establish the generality of the proposed design principle. Attributing inner-layer formation to LiDOB or LiNO3 decomposition based solely on Li2O detection is unconvincing, as Li2O can also result from the decomposition of imide-based salts such as LiFSI or LiTFSI. This overlap in decomposition pathways limits the interpretability of the experimental evidence. Without further mechanistic clarification, the claim of a general design principle remains premature.

Reviewer #2

(Remarks to the Author)
I have no more questions.

Reviewer #3

(Remarks to the Author)
The authors provide detailed response to the reviewer's comment. The "voltage-driven anion migration" strategy was further discussed in details in the revised manuscript, which may promote the development of phosphate electrolyte. Some remaining points need to be addressed.

1. The experimental evidence of dual-layer SEI is not convincing. XPS was used in the manuscript to verify the dual-layer feature of SEI, which is a key finding of this work. However, XPS results can be misleading sometime, where the sputtering is not homogeneous among different components, undermining the claim of dual-layer SEI formation. To clearly demonstrate the dual-layer feature of SEI, cryogenic electron characterization is suggested.

2. The applicability of the so-called "voltage-driven anion migration" strategy in Li metal full cell should be fully charified. This manuscript reports a voltage-based strategy to regulate SEI. However, it is known that Li chemically reacts with electrolyte to form an SEI before cycling, i.e., before applying the electric field. Such a chemically formed SEI may substantially affect the "voltage-driven anion migration" strategy to regulate the SEI structure. The compasion between reported electrolyte and traditional carbonate electrolyte is not very convincing.

3. The FTIR results need more detailed discussion. Please provide references for each peak's attribution in the profiles. In particular, the peak position of LiF needs to be checked. Meanwhile, the curve change during charge and discharge process is not very clear, since most of curves overlap in Fig. 2a.

4. The formation mechanism of dual-layer SEI remains not very clear. It was found that DFOB- can be decomposed to form B-O species in the inner SEI. In principle, DFOB- can decompose to form LiF in the meantime, but the inner SEI lacks LiF. Why can't we detect large amount of LiF in the inner layer?

5. In Fig. 1f, it can be seen that the solvent TEP dominates on the Li surface. Since all of electrolyte components, including TEP, BF4-, DFOB- and NO3-, can decompose on Li surface, more TEP corresponds to more severe TEP decomposition. How can those minor species (anions) on Li surface can protect Li metal from reactive phosphate?

Version 2:

Reviewer comments:

Reviewer #1

(Remarks to the Author)
I thank the authors for their comprehensive revisions and additional analyses, which have considerably strengthened the manuscript. In addition, I would ask the authors to address the following points.

1. The finding that OPLS-AA can describe the interaction between Li metal and Li ions with accuracy comparable to DFT is indeed surprising. Could the authors clarify whether the Lennard–Jones parameters for Li metal were specifically adjusted in this work, or whether they were taken directly from previous literature? For the sake of reproducibility and transparency, it is essential that the full set of Lennard–Jones parameters used in the simulations be included in the Supplementary Information. Furthermore, the computational details of the DFT calculations performed for validation are not currently provided in the Supplementary Information. These details must be explicitly included to allow the results to be properly assessed and reproduced.

2. I remain unconvinced by the manuscript's conclusion that differences in anion adsorption strength within 1 nm of the Li

metal surface directly determine the SEI structure extending over tens of nanometers. Even if the adsorbed anions decompose during the initial stages of SEI formation, subsequent processes such as ion transport are also involved in SEI growth. Therefore, it does not seem reasonable to directly link the initial local adsorption state to the final SEI architecture. A clear rationale is required to bridge this scale gap and substantiate the proposed mechanism.

Minor comment: Please change the frame color in Fig. S29b to yellow.

Reviewer #3

(Remarks to the Author)
This reviewer has no other questions. The revised manuscript can be published.

Version 3:

Reviewer comments:

Reviewer #1

(Remarks to the Author)
The authors have adequately addressed my previous concerns. The manuscript is now suitable for publication.

Thank you for your email informing us of your editorial decision on our manuscript (NCOMMS-25-16384A). According to the instructions in your email, we have carefully considered the helpful criticism from the referees and revised the manuscript accordingly. We provide a detailed response to the referees' criticism below. The changes made during revision are highlighted in yellow and the file is uploaded separately for review only.

Reviewer #1 (Remarks to the Author):

This manuscript presents an electrolyte formulation by mixing three different lithium salts with a flame-retardant solvent. The authors claim that the proposed electrolyte exhibits superior electrochemical properties compared to a conventional 1 M $LiPF_6$/EC-DMC electrolyte, attributing this enhancement to the cooperative effect of the three anions in forming a robust protective layer on the electrode surface. However, the manuscript contains numerous deficiencies, with significant shortcomings in the analysis used to support its conclusions. Consequently, the reviewer finds that this work does not meet the high standards of Nature Communications. The key issues are as follows:

Response: Many thanks for the referee's valuable suggestion, especially, the insightful comments for further improving the quality of the manuscript. We have carefully addressed the issues as follows.

1. The manuscript adopts 1 M $LiPF_6$/EC-DMC as the benchmark electrolyte. However, it is well known that this electrolyte undergoes severe degradation when paired with a lithium metal anode. This choice appears to be a deliberate attempt to exaggerate the

performance of the proposed electrolyte. To substantiate the claim of superior performance, a comparison should be made against state-of-the-art imide-based electrolytes.

Response: We deeply appreciate the reviewer's meticulous assessment and insightful feedback. We selected the commercial $LiPF_6$/EC-DMC electrolyte as the baseline because it has been widely adopted in the industry and serves as a standard reference for evaluating electrolyte performance. To further investigate the effects of different electrolyte systems, we also conducted comparative experiments using lithium sulfonylimide-based electrolytes, as suggested. These systems include 1.5 M LiFSI/TEP, 1.5 M LiTFSI/TEP, 1.5 M LiFSI/EC-DMC, and 1.5 M LiTFSI/EC-DMC.

Our findings revealed that all four systems suffered from inadequate cycling performance. Specifically, 1.5 M LiFSI/EC-DMC exhibited voltage stagnation during the initial charge, likely due to severe oxidative decomposition (Figure caption1a). Although 1.5 M LiTFSI/EC-DMC completed charge–discharge cycles, it rapidly lost capacity within 100 cycles (Figure caption1b). Both 1.5 M LiFSI/TEP and 1.5 M LiTFSI/TEP electrolytes delivered low initial capacities and experienced rapid capacity decay (Figure caption1c and d).

These observations suggest that LiTFSI and LiFSI electrolytes promote aluminum current collector corrosion: $TFSI^-$ ions aggressively attack the Al_2O_3 layer, causing localized pitting (*Nat Commun* ***15****, 2922 (2024)*), while FSI^- ions at high voltages promote AlF_3 formation and induce mechanical failure within the passivation layer (*Journal of Applied Electrochemistry* ***29****, 1053–1061 (1999)*). Moreover, LSV analyses indicated that the oxidation thresholds of these electrolytes are below 4.8 V, inherently limiting their high-voltage compatibility and contributing to poor overall electrochemical performance (Figure caption1e).

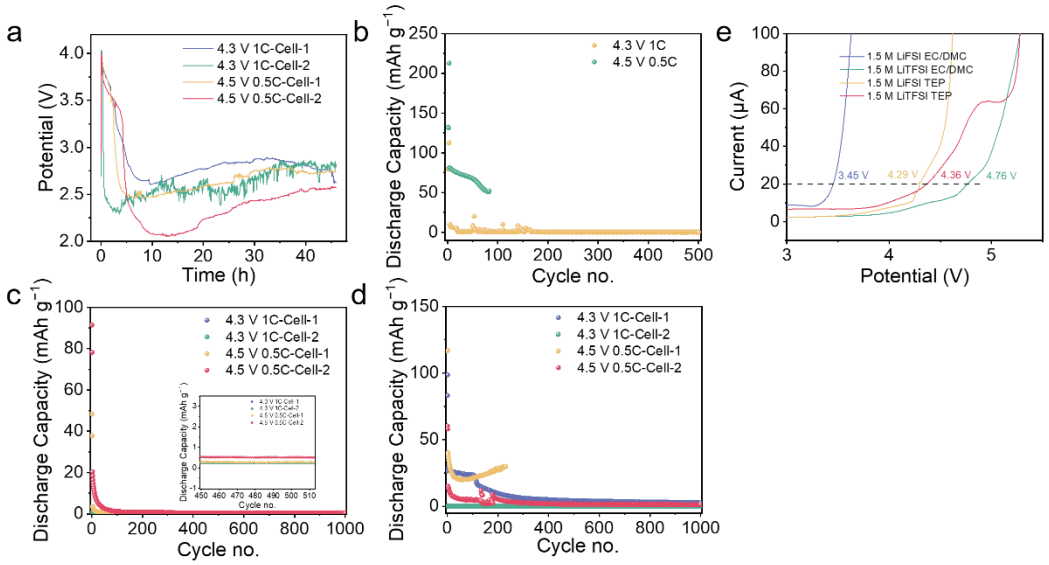

Figure caption1. (a) Time–voltage profile of the first cycle for the 1.5 M LiFSI/EC-DMC electrolyte. (b) Cycling performance of the 1.5 M LiTFSI/EC-DMC electrolyte under 4.3 V 1C and 4.5 V 0.5C conditions. (c) Cycling performance of the 1.5 M LiFSI/TEP electrolyte under 4.3 V 1C and 4.5 V 0.5C conditions. (d) Cycling performance of the 1.5 M LiTFSI/TEP electrolyte under 4.3 V 1C and 4.5 V 0.5C conditions. (e) Linear sweep voltammetry (LSV) curves of the four electrolytes.

2. The study employs molecular dynamics simulations of the Li electrode–electrolyte interface under an applied electric field, yet several methodological issues undermine the reliability of these calculations. First, the interaction between lithium metal and the electrolyte cannot be accurately described using a standard classical force field (OPLS-AA), as it severely underestimates adsorption strength compared to first-principles calculations. Additionally, an excessively high electric field (-1.0 V/nm) is applied to the electrode surface, leading to an unrealistic accumulation of Li ions at the interface, which likely affects the anion distribution as well. Since the proposed mechanistic interpretation relies solely on simulation results, further efforts are required to ensure an accurate representation of ion distributions at the Li metal surface.

Response: We sincerely thank the reviewer for their thorough evaluation of our work. The reviewer correctly pointed out that the OPLS-AA force field may have certain limitations in describing the interactions at the lithium metal/electrolyte interface. However, the main objective of this study is to investigate the migration behavior of anions in the electrolyte under realistic operating voltages, rather than to accurately model interfacial behavior between lithium metal and the electrolyte. Therefore, the use of the OPLS-AA force field remains appropriate and justified for the purpose of this work.

We thank the reviewer for their insightful comments regarding the electric field strength (−1.0 V/nm) used in our simulations. We acknowledge that this value exceeds the typical electric field strengths encountered under experimental conditions. However, as commonly adopted in molecular dynamics (MD) simulations (see RSC Adv., 2018, 8, 5255–5267; Phys. Chem. Chem. Phys., 2023, 25, 23937–23953; Advanced Powder Materials, 2025, 100296), the application of a relatively high electric field is a necessary strategy to achieve statistically significant results within the limitations of finite simulation boxes and nanosecond timescales. It is important to emphasize that while the absolute magnitude of the field is elevated, it does not compromise the core conclusion of our study—that is, the relative migration behavior of different anions under an applied electric field, which remains the central scientific question addressed in this work.

We sincerely thank the reviewer for their insightful and thorough evaluation of our study. We fully understand the reviewer's concern regarding the mechanistic explanation being primarily based on theoretical simulations. In fact, our investigation is built upon a tightly integrated framework that combines both theoretical modeling and extensive experimental validation. In our preliminary literature review, we observed that different lithium salt anions exhibit significantly varied binding energies with Li^+—for instance, LiODFB and LiBOB show stronger binding affinities, while $LiBF_4$ and $LiPF_6$ exhibit relatively weaker interactions. This observation inspired us to

investigate how such disparities manifest in practical battery systems. Through molecular dynamics (MD) simulations, we found that these binding energy differences indeed influence the migration behavior of anions. Strongly coordinating anions such as NO_3^- and $ODFB^-$ tend to migrate in conjunction with Li^+ toward the anode interface, thereby theoretically favoring the formation of an inner SEI layer enriched with Li_3N and B–O species. In contrast, weakly coordinating anions like BF_4^- tend to remain further from the electrode surface, contributing instead to the formation of a LiF-rich outer SEI. To experimentally confirm this SEI formation mechanism, we employed in situ infrared spectroscopy. As shown in Figures 2a and S16, we quantitatively analyzed the interfacial behavior of surface anions by comparing the ratios of characteristic peak areas at the end of lithium deposition and during the stripping stage. Notably, PF_6^- (which has a weaker coordination with Li^+) exhibited significantly higher reversibility, while $ODFB^-$ underwent more pronounced consumption, indicating its stronger participation in interfacial reactions (Figure 2b). This result is consistent with our theoretical calculations and supports the hypothesis that the stronger binding affinity of $ODFB^-$ facilitates its migration toward the lithium surface, where it undergoes intensive decomposition and contributes to the formation of the inner SEI layer. Subsequently, we employed X-ray photoelectron spectroscopy (XPS) and time-of-flight secondary ion mass spectrometry (TOF-SIMS) to validate the predicted compositional distribution within the SEI. To further probe the nanoscale structure of the solid electrolyte interphase, we performed sputtering XPS analysis on the Li||NCM811 interface after 100 cycles. As illustrated in the F 1s spectrum (Figure 2a), LiF is predominantly distributed in the outer SEI. In contrast, the B 1s and N 1s spectra exhibit broader and more intense peaks for B–O and Li_3N species with increasing sputtering time, indicating their localization within the inner SEI (Figures 2b–c). To further elucidate the spatial distribution of the triphasic SEI formed in the 0.5 M-DBN electrolyte, TOF-SIMS analysis was conducted to visualize the structural evolution of the lithium anode in three dimensions (Figures 2h-i). Interestingly, LiF species were found primarily in the outer SEI layer, whereas Li_3N and B–O components were concentrated in the inner region. In summary, our proposed mechanism is supported by a coherent and robust

chain of evidence—from theoretical predictions to systematic experimental validation—demonstrating the rationality and reliability of our mechanistic model.

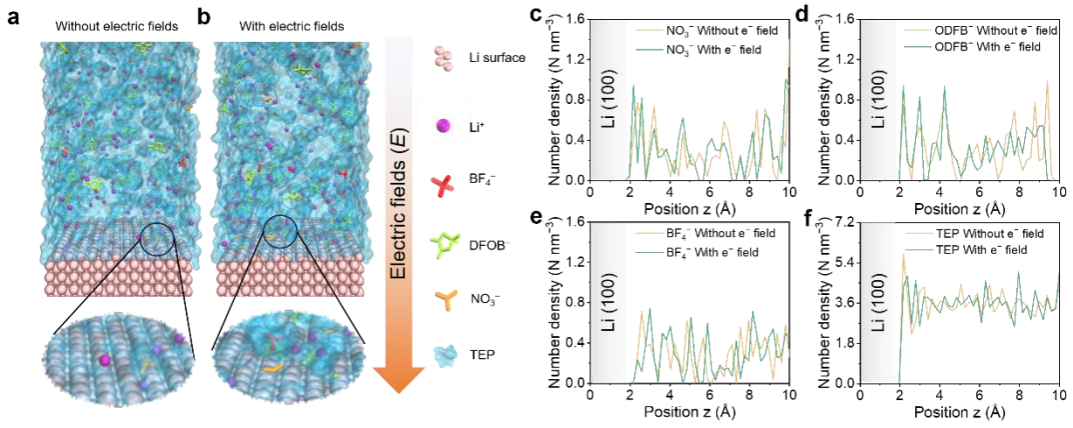

Figure 1a-f. Snapshots of the lithium-metal-anode-electrolyte interfacial system without (a) and with (b) an electric field. The large arrow indicates the direction of the external electric field. Quantity distribution in the z-direction for each substance. (c)NO_3^-, (d)$ODFB^-$, (e)BF_4^- and (f)TEP.

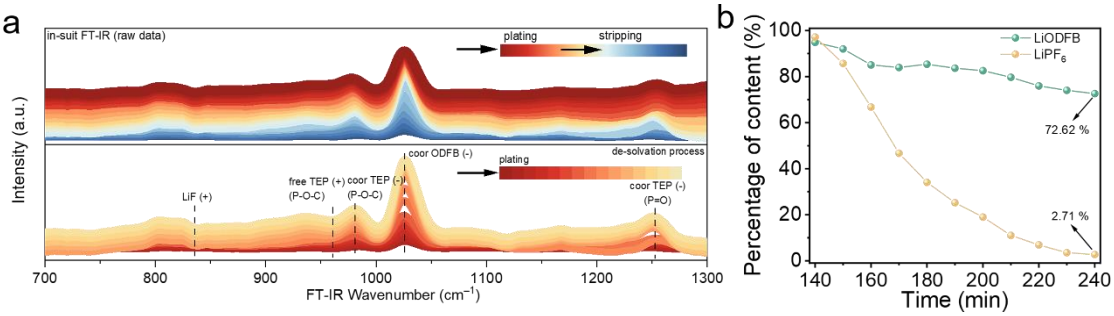

Figure 2a-b. Contour plots of In-suit Fourier-transform Infrared (FTIR) spectra of the electrode/electrolyte interfaces in a 0.5 M-DBN electrolyte (a) and their content variations (b).

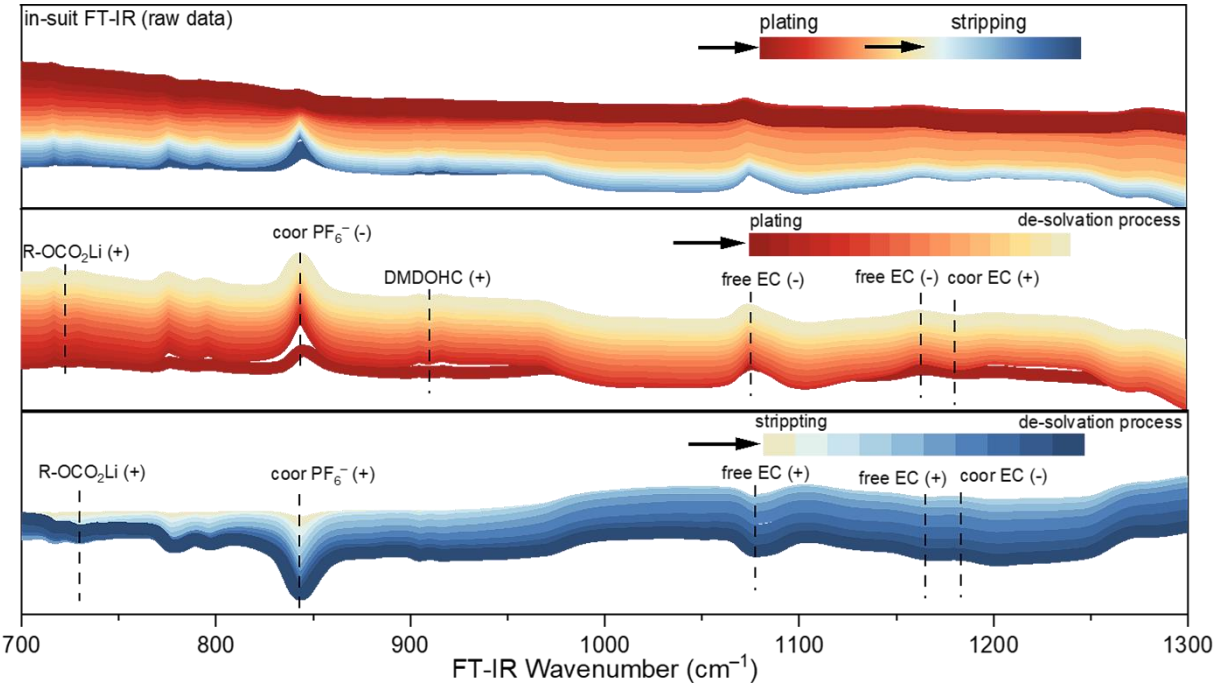

Figure S16. Contour plots of Fourier-transform infrared (FTIR) spectra of the electrode/electrolyte interfaces in a 1 M $LiPF_6$ EC/DMC.

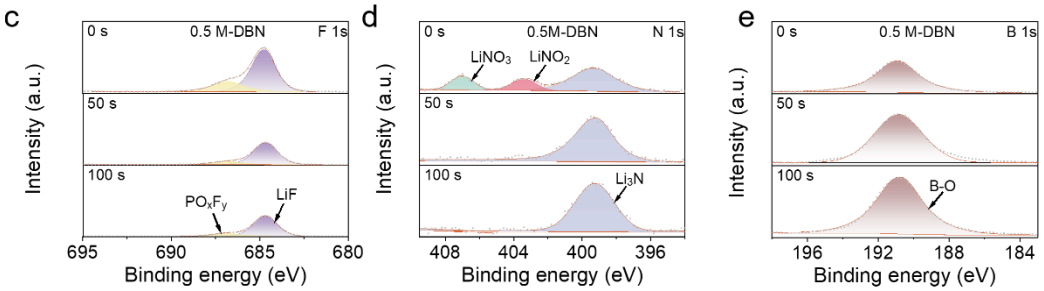

Figure 2c-e. XPS depth profiles were determined of (c) F1s, (d) N1s, and (e) B1s of lithium metal anodes recovered from full cell cycled with 0.5 M-DBN electrolyte at sputtering times of 0, 50, and 100 s, respectively.

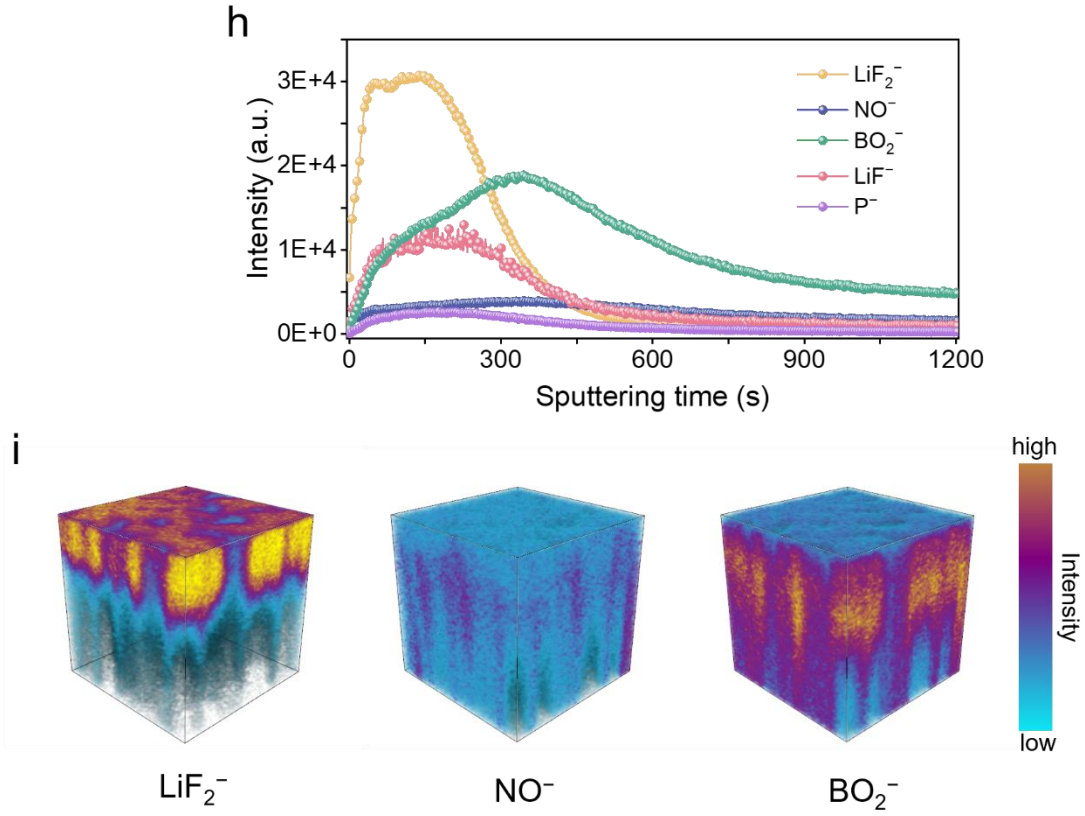

Figure 2h-i. Time-of-flight Secondary Ion Mass Spectrometry (TOF-SIMS) depth distributions (h) and three-dimensional images of various species (i) within a 0.5 M-DBN electrolyte.

3. The proposed mechanism is based on differences in ion distributions within a sub-nanometer scale. However, the spatial scale of the solid electrolyte interphase (SEI) typically ranges from 10 to 100 nm. Thus, the claim that such minor initial variations directly translate into the experimentally observed SEI composition lacks sufficient justification.

Response: We are grateful to the reviewer for the constructive comments and for highlighting critical questions regarding our proposed mechanism. The reviewer rightly noted that our mechanism fundamentally depends on the nanoscale modulation of interfacial ion distribution. This mechanism relies on the variation in binding energy between lithium ions (Li^+) and different anions, specifically $ODFB^-$, NO_3^-, and BF_4^-. Due to the significantly higher binding energies of Li^+ with $ODFB^-$ and NO_3^- compared to BF_4^-, Li^+ tends to migrate alongside $ODFB^-$ and NO_3^- under the influence of an electric field, resulting in their accumulation near the lithium metal surface. In contrast, BF_4^-, with its weaker binding, remains more dispersed and distant from the interface. This distinct spatial distribution of ions dynamically shapes a gradient-structured solid electrolyte interphase (SEI), where the inner layer is enriched with B – O bonds and Li_3N, while the outer layer primarily consists of LiF. We would like to emphasize that this effect is not restricted to the initial stages but persists throughout battery operation. Since the electrolyte consistently contains all three anions and the electric field continuously drives ion migration, the selective distribution process remains active throughout. As shown by the in-situ infrared spectroscopy in Figures 2a-b and S18, LiODFB is continuously and irreversibly consumed on the copper current collector side during the discharge stage. Therefore, the binding-energy-driven distribution plays a sustained and pivotal role in steering the long-term evolution of SEI composition and structure. We thank the reviewer again for enhancing the rigor of our explanation.

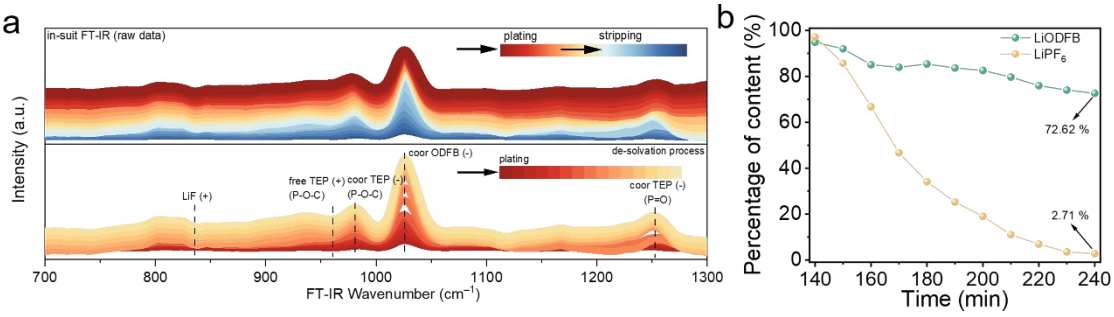

Figure 2a-b. Contour plots of In-suit Fourier-transform Infrared (FTIR) spectra of the electrode/electrolyte interfaces in a 0.5 M-DBN electrolyte (a) and their content variations (b).

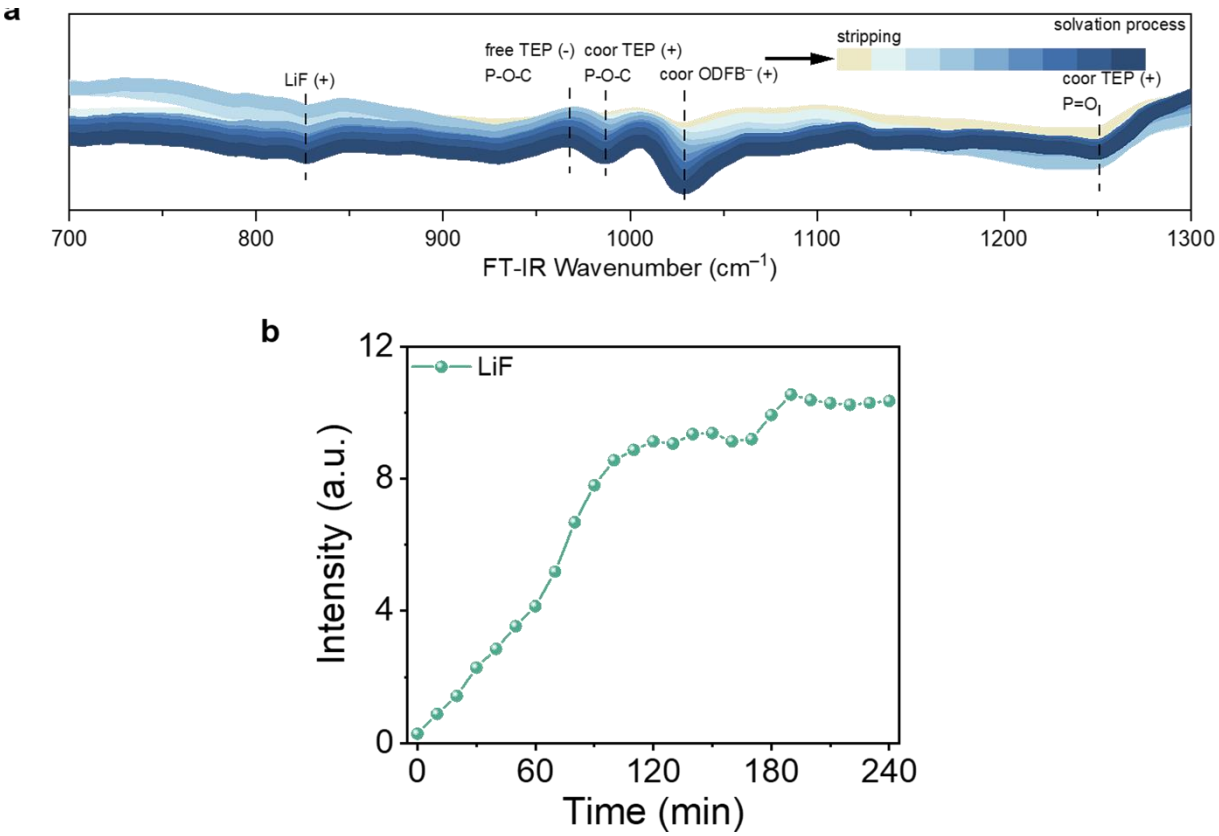

Figure S18. (a) Contour plots of Fourier-transform infrared (FTIR) spectra of the electrode/electrolyte interfaces in a 0.5 M-DBN. (b) LiF content variation in in situ FTIR.

4. $LiNO_3$ is widely recognized as an additive that stabilizes the SEI layer, improving both film stability and battery lifespan. The inclusion of $LiNO_3$ in the electrolyte and its reported effects do not present a novel finding.

Response: We sincerely thank the reviewer for the careful and thoughtful review of our manuscript. As the reviewer rightly pointed out, the addition of $LiNO_3$ and its effect on SEI formation has been previously reported and is not itself a novel finding. However, the novelty of our work lies not in the use of $LiNO_3$ as an additive, but in the interfacial regulation mechanism we propose, which is based on the binding energy

differences between Li^+ and various anions. Specifically, our key finding is that Li^+ exhibits significantly stronger binding with $ODFB^-$ and NO_3^- than with BF_4^- (Li^+–$ODFB^-$/NO_3^- > Li^+–BF_4^-), which leads to a spatially selective distribution of anions under an applied electric field. That is: (1) $ODFB^-$ and NO_3^-, with stronger binding energies, tend to co-migrate with Li^+ and accumulate near the lithium metal surface; (2) BF_4^-, with weaker binding, remains away from the electrode interface. This dynamic ion distribution enables the formation of a gradient SEI structure—an inner layer rich in B–O bonds and Li_3N, and an outer layer primarily composed of LiF. This mechanism is fundamentally different from previously reported approaches that rely solely on the addition of $LiNO_3$ (*e.g., Angew. Chem. Int. Ed. 2022, 61, e202206682; Angew. Chem. Int. Ed. 2025, 64, e202410020*), where the effect of the additive is not driven by competitive ion distribution. In contrast, our work introduces a new design concept based on binding-energy-driven ion selection, offering a theoretical foundation and practical strategy for precise interfacial engineering in lithium metal batteries. We appreciate the reviewer's comments, which helped us to clarify the innovation of our study.

5. If the cooperative effect of three anions is to be claimed as a central finding, it is necessary to consider a broader range of anionic species to evaluate the generality of the proposed mechanism. Without such validation, the novelty of the proposed strategy remains questionable.

Response: We sincerely appreciate the reviewer's thorough evaluation of our study. As rightly pointed out, the original manuscript did not adequately address the generality of different anions. In the revision, we we conducted two additional control experiments to validate the broader applicability of our proposed strategy according to the reviewer's suggestion:

In the first set, a 0.5 M LiBOB + 0.5 M LiFSI TEP-based electrolyte was employed (LiBOB exhibits a higher binding energy than LiFSI). According to our theoretical predictions, LiBOB is expected to reside closer to the lithium surface and preferentially decompose, forming a B–O-rich inner SEI layer, while the weaker-binding LiFSI contributes to a LiF-rich outer SEI. Sputtering XPS analysis of the SEI composition (Fig. X) fully confirms the presence of this layered structure.

In the second set, a 0.5 M $LiNO_3$ + 0.5 M LiTFSI TEP electrolyte was used ($LiNO_3$ has a higher binding energy than LiTFSI). Theoretical predictions suggest that $LiNO_3$ preferentially decomposes on the Li surface, forming a Li_2O-rich inner SEI (Li_2O was selected as a marker to exclude the influence of nitrogen from LiTFSI), while LiTFSI forms a LiF-dominated outer SEI. Sputtering XPS results (Fig. Y) again confirm this spatial distribution.

These findings collectively demonstrate that the anion gradient distribution mechanism we proposed is not a system-specific phenomenon, but rather a general interfacial regulation principle. This discovery offers critical theoretical support for designing high-performance SEIs via strategic anion selection. Please refer to the description in lines 223–226 of the manuscript: *"Meanwhile, experimental verification using other combinations of strong and weak coordinating lithium salts further revealed the same SEI formation pattern, confirming the universality and effectiveness of this strategy (Fig. S15)."*

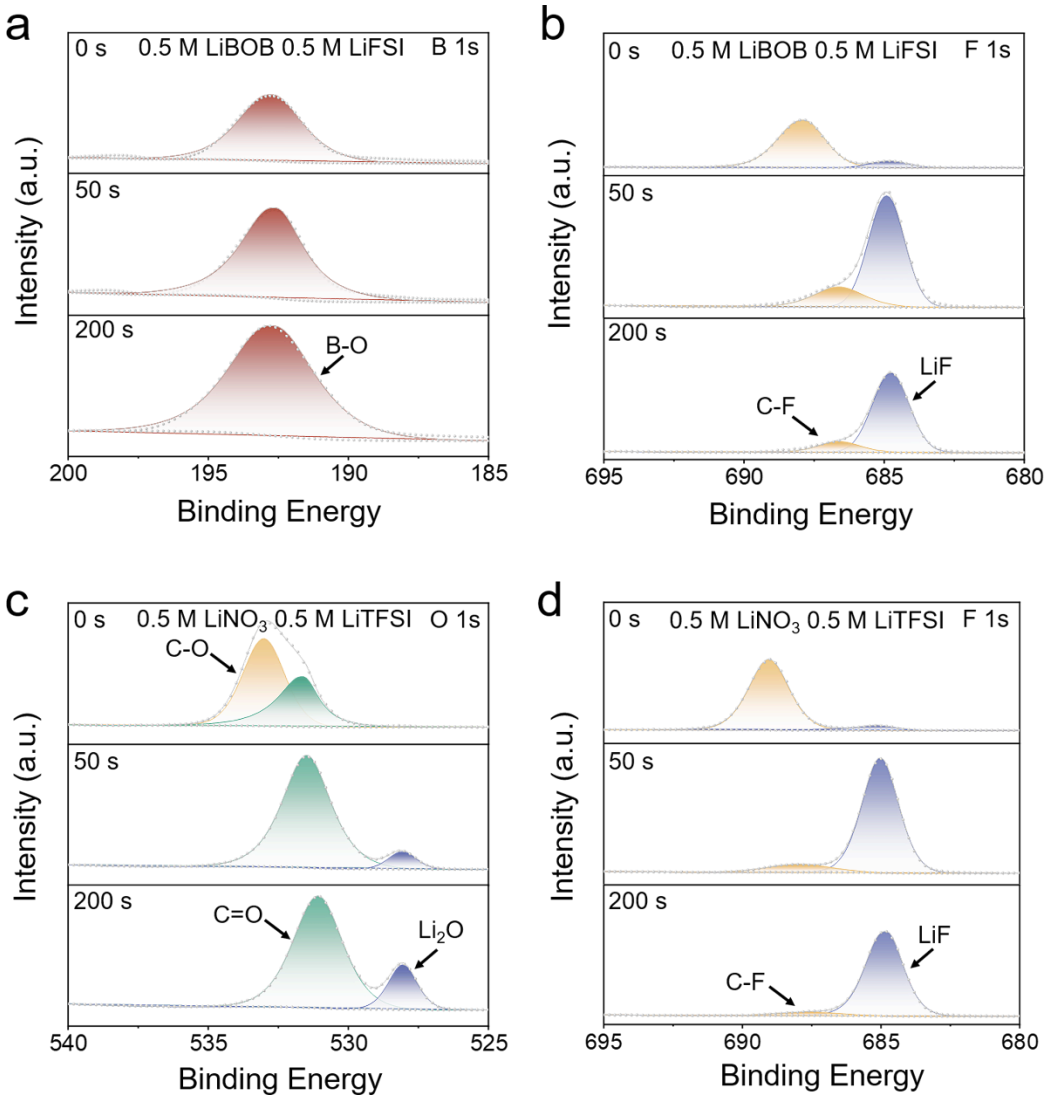

Figure caption (a) B1s and (b) F1s XPS spectra of the SEI formed in the 0.5 M LiBOB + 0.5 M LiFSI TEP electrolyte. (c) O1s and (d) F1s XPS spectra of the SEI formed in the 0.5 M $LiNO_3$ + 0.5 M LiTFSI TEP electrolyte.

Reviewer 2

1. The article is interesting, and reveals a layered SEI formed by ternary lithium salts: an inner layer composed of Li_3N and B-O, and an outer layer of LiF, achieving a comprehensive performance of high ionic conductivity, mechanical strength, and toughness for the SEI. The results in the manuscript are very meaningful for the development of lithium metal batteries, and I would like to try a industrial demo according to the reported cell design after the manuscript, of course, will be published.

Response: Many thanks for your very positive evaluation on the topic of our research and the support for publication, especially, the constructive comments and insightful suggestions for further improving the quality of the manuscript.

2. According to the results of the radial distribution function, regardless of whether an electric field is applied, TEP still predominates on the lithium metal surface. Following the authors' design logic, higher lithium salt concentrations may result in better SEI formation efficiency. The understanding of the optimized 0.5 M-DBN should be addressed.

Response: We sincerely thank the reviewer for taking the time to read our manuscript and for the valuable comments. As the reviewer insightfully pointed out, TEP (triethyl phosphate) dominates the interfacial layer on the lithium metal surface regardless of the presence of an applied electric field. This observation can be attributed to the overwhelming molar ratio of TEP in the electrolyte composition. As shown in Table S1, the TEP content reaches 5.9 mmol per 1 mL of electrolyte, while the total concentration of the three lithium salts (LiODFB, $LiBF_4$, and $LiNO_3$) is only 0.5 mmol. However, despite its quantitative dominance, TEP exhibits a significantly higher LUMO energy level (Figure 1i) compared to the anions of the lithium salts. This electronic structure feature ensures that the lithium salts are preferentially reduced over TEP, leading to an SEI film that is predominantly composed of lithium salt decomposition products rather than solvent-derived species. Regarding the reviewer’s comment on the relationship

between lithium salt concentration and SEI formation efficiency, we fully agree that a higher salt concentration can enhance the formation of the SEI. Nevertheless, we emphasize that excessively high concentrations introduce two key drawbacks: (1) a decrease in ionic conductivity and (2) a substantial increase in viscosity, both of which severely impair ion transport in the electrolyte. Our systematic screening experiments (Figure S1) demonstrate that under a fixed salt ratio (LiODFB: $LiBF_4$: $LiNO_3$ = 1:1:1, mol/mol/mol), the 0.5 M DBN-based electrolyte exhibits the highest ionic conductivity (5.13 mS/cm). Further increasing the concentration does not improve performance; on the contrary, it leads to reduced conductivity and ultimately degrades the cycling stability of the battery.

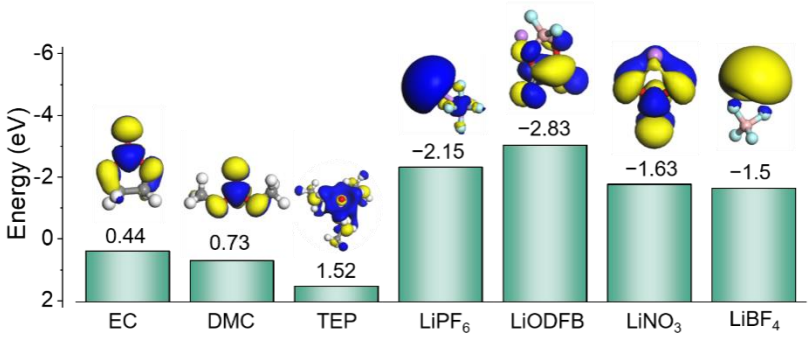

Figure1i. LUMO energy of neutral of EC, DMC, TEP, $LiPF_6$, LiODFB, $LiNO_3$, $LIBF_4$.

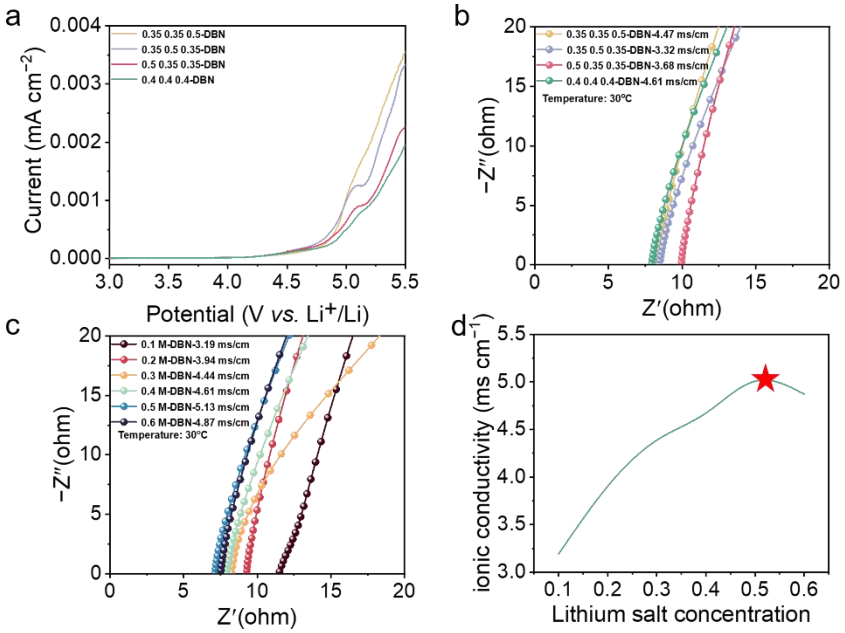

Figure S1. Systematic screening of the electrolyte formulation with an optimum ratio. (a) Oxidative stability of various electrolytes in various proportional formulations at a total concentration of 1.2 M. (b) Ionic conductivity of various electrolytes in different proportions of formulations with a total concentration of 1.2 M. (c) The Nyquist plots of XMol-DBN electrolytes. (d) The Li^+ conductivity of XMol-DBN electrolytes.

Table S1. Detailed components of the four MD models

Components	TEP (mmol)	LiODFB (mmol)	$LiBF_4$ (mmol)	$LiNO_3$ (mmol)
0.5 M LiODFB+0.5 M $LiBF_4$ +0.5 M $LiNO_3$ in TEP	5.9	0.5	0.5	0.5

Molecule number	589.0	50.0	50.0	50.0

3. In line 165, "electrical conductivity" is suggested to be more accurately changed to "ionic conductivity".

Response: We thank the reviewer for the careful review of our manuscript. In response to the reviewer's suggestion, we have revised the sentence at line 165 of the manuscript as follows: *"Due to the low ionic conductivity of SEI, the transport of lithium ions is hindered, resulting in uneven deposition on the surface of the lithium anode, and ultimately the formation of lithium with highly porous morphology and whisker structure."*

4. The experiment uses the electrolyte of $LiPF_6$/carbonate as the reference, while the electrolyte of TEP/three salts is a completely different recipe. It would be more convincing if a comparison of carbonate/three salts with $LiPF_6$/carbonate will be adopted.

Response: We sincerely thank the reviewer for the thorough evaluation of our manuscript. Due to the extremely low solubility of lithium nitrate in commercial carbonate solvents (approximately 0.01 mg/mL), these solvents were not used as the electrolyte medium in this study. In response to the reviewer's comment, we prepared a control electrolyte composed of 0.75 M LiODFB/EC-DMC and 0.75 M $LiBF_4$/EC-DMC(note that $LiNO_3$ could not be dissolved in the EC/DMC solvent system and was

therefore not included in the control formulation). Comparative experiments were conducted under two different testing conditions: 4.3 V at 1C and 4.5 V at 0.5C.

As shown in the figures caption2, under the 4.3 V 1C condition, the 0.5 M-DBN electrolyte exhibited excellent cycling stability, retaining 87.90% of its initial capacity after 900 cycles. In contrast, the 0.75 M LiODFB + 0.75 M $LiBF_4$ EC/DMC electrolyte retained only 36.97% of its capacity. Under the higher voltage condition (4.5 V), the 0.5 M-DBN electrolyte still maintained 90.91% capacity retention after 600 cycles. These comparative results clearly demonstrate the superior cycling performance of the 0.5 M-DBN electrolyte.

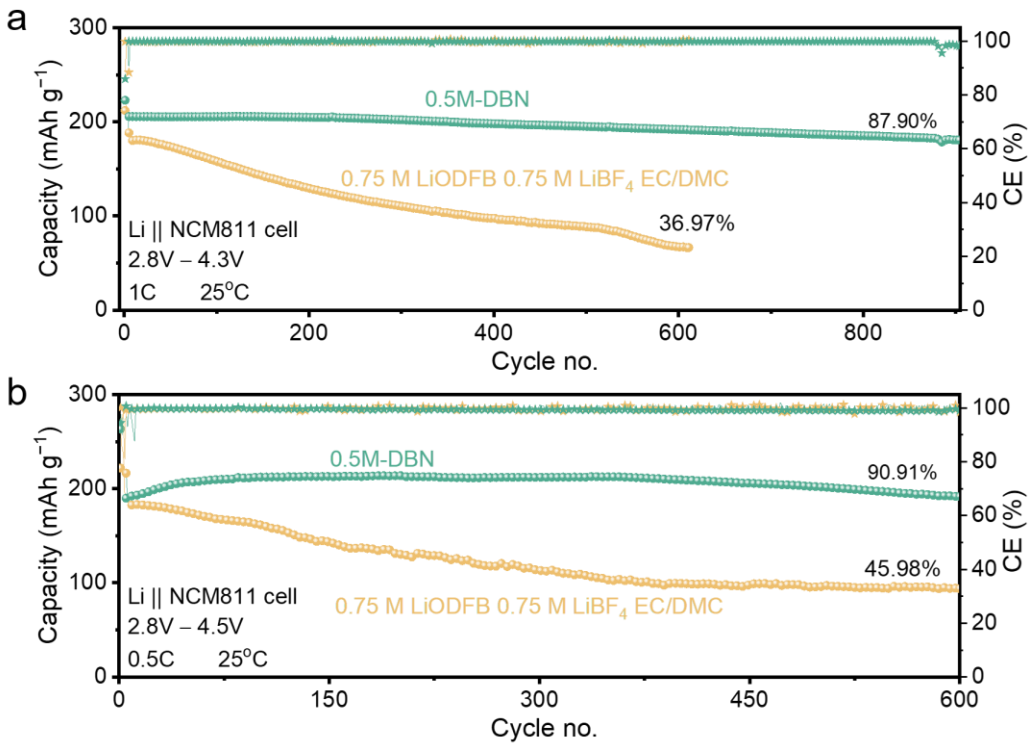

Figure caption2. Comparison of the cycling performance of the two electrolytes under (a) 4.3 V at 1C and (b) 4.5 V at 0.5C conditions.

5. It is unclear that the first appearance of 1.5 M-N in line 171 while its explanation is in line 213. This should be revised for clarity.

Response: We thank the reviewer for the thorough review of our manuscript. In accordance with the reviewer's suggestion, we have revised the description of the 1.5 M-N electrolyte and relocated it to the appropriate position at line 171. The revised text is as follows: *"Average DMT of as-formed B-O-rich SEI films by 0.5 M-DBN electrolyte was 2.12 GPa, which was 1.44 times higher than that of SEI films formed by the 1.5M-N (1.5 mmol of $LiNO_3$ of TEP, noted as 1.5 M-N) electrolyte (the average DMT of 1.5 M-N was 1.47 GPa) (Figure 2f and S19)."*

6. Are the three salt concentrations in 0.5-DBN all 0.5 mol? The 1.5M-N electrolyte is noted later as 1.5 mmol, which makes the comparison of SEI strength in line 171 meaningless.

Response: We sincerely thank the reviewer for the careful and detailed review of our manuscript. In response to the comment, we have revised the description of the 1.5 M-N electrolyte at line 171 to explicitly state that its total lithium salt concentration is 1.5 mol L^{-1}. Additionally, as noted at line 89, the total lithium salt concentration of the 0.5 M-DBN electrolyte is also 1.5 mol L^{-1}. This consistency in concentration ensures the scientific validity of the SEI performance comparison. The revised sentence in the manuscript now reads as follows: *"Average DMT of as-formed B-O-rich SEI films by 0.5 M-DBN electrolyte was 2.12 GPa, which was 1.44 times higher than that of SEI films formed by the 1.5M-N (1.5 mmol of $LiNO_3$ of TEP, noted as 1.5 M-N) electrolyte (the average DMT of 1.5 M-N was 1.47 GPa) (Figure 2f and S19)."*

7. In line 212, is the salt concentration also in mmol? Comparing to the total salt concentration of 1.5 mol in 0.5M-DBN, it is also not appropriate.

Response: We thank the reviewer for the careful evaluation of our manuscript. In response to the suggestion, we have standardized the concentration units for all electrolyte formulations throughout the manuscript, replacing the original millimole (mmol) expressions with molar (M) units. The revised description at line 213 now reads as follows: *"For comparison, CE of cycling with the 0.75 M-DB (0.75 M LiODFB and $LiBF_4$ of TEP, noted as 0.75 M-DB), 1.5 M-N, and 1M $LiPF_6$ EC/DMC electrolytes were approximately 91.45%, 87.05%, and 84.52%."*

8. Figure S1b shows that the ionic conductivity of 0.4 M-DBM is 4.92 mS/cm, but in Figure S1c, the ionic conductivity of 0.4 M-DBM is shown as 3.86 mS/cm. Please confirm the actual ionic conductivity of the electrolyte.

Response: We sincerely thank the reviewer for the detailed and constructive comments. In response, we have re-measured the ionic conductivity of all electrolyte samples, including 0.4 M-DBN, using the same batch of cells under identical experimental conditions. The corrected data (presented in Supporting Information Figure S1) show good consistency across all samples. We sincerely apologize for the data deviation caused by previously inconsistent testing conditions. The updated results further support the reliability of the original conclusions.

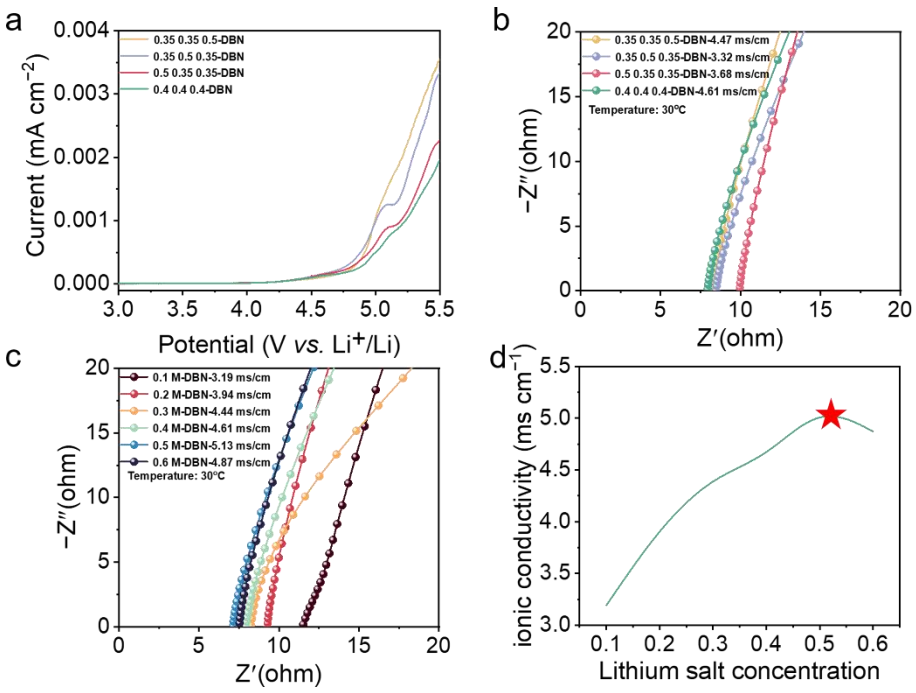

Figure S1. Systematic screening of the electrolyte formulation with an optimum ratio. (a) Oxidative stability of various electrolytes in various proportional formulations at a total concentration of 1.2 M. (b) Ionic conductivity of various electrolytes in different proportions of formulations with a total concentration of 1.2 M. (c) The Nyquist plots of XMol-DBN electrolytes. (d) The Li^+ conductivity of XMol-DBN electrolytes.

A comprehensive comparison of the oxidative stability and Li^+ conductivity of different electrolytes with different ratio formulations, with a total concentration of 1.2 M in (a) and (b), revealed that the electrolyte with a lithium salt ratio of 1:1:1 exhibited the most promising results. Further comparison of the Li^+ conductivity of the XM-DBN electrolyte revealed that 0.5M-DBN was selected as the optimal electrolyte formulation.

9. In Figure 2a, there is a typo in "In-suit Fourier-transform Infrared (FTIR) spectra". The spectra provided in the article are difficult to be interpreted in terms of the trends of the signal peaks. It would be more helpful to present the data as Contour plots.

Response: We sincerely thank the reviewer for the important suggestion regarding data visualization. As rightly pointed out, contour plots can offer advantages in illustrating the trends of spectral features. However, the in situ infrared data obtained in our study may not be well-suited for contour representation due to baseline inconsistencies across different time points. As shown in Figure 10, the initial segment of the data (highlighted by the dashed box) exhibits notably different baseline levels. If plotted as contour maps, these inconsistencies could mask subtle but important features, such as the LiF-related peak at 833 cm^{-1}. Although we have performed minimal baseline correction using the lowest intensity as reference, further aggressive normalization to force all spectra onto a unified baseline would distort peak intensities and potentially compromise the reliability of the results. Moreover, as demonstrated in Figure 11, we have attempted to generate a contour plot for the in situ infrared data. Notably, due to the aforementioned baseline variations, downward-directed generation peaks could not be accurately captured, further limiting the effectiveness of this approach.

In contrast, the line plots we used are better suited for preserving the integrity of the original data. They clearly present intensity differences over time, capture the evolution of negative peaks, and effectively reveal trends in weaker spectral features. Particularly for analyzing how individual peak shapes change over time, line plots offer superior resolution and clarity.

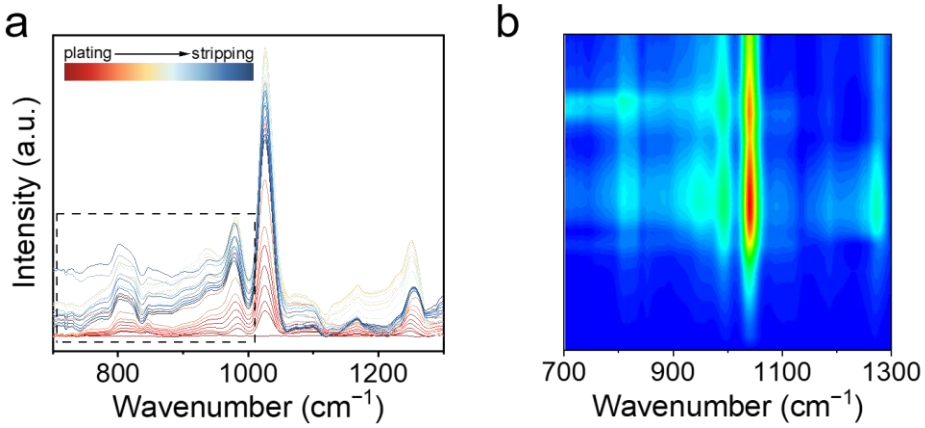

Figure caption 3. (a) Stacked in situ infrared spectra of the 0.5 M-DBN electrolyte. (b) Contour plot of the in situ infrared spectra for the 0.5 M-DBN electrolyte.

10. The initial discharge capacity of 2.8-4.5 V (Figure 5b & Figure S39) at 0.5 C is lower than that of 2.8-4.3 V (Figure 5a) at 1 C. How to understand?

Response: We sincerely thank the reviewer for the careful review of our manuscript and the valuable comments. Regarding the mechanism underlying this phenomenon, we acknowledge that it may involve the coupling of multiple factors. However, we believe that the most critical factor is a partially reversible structural transformation of the cathode material during cycling. Both theoretical analysis and experimental evidence suggest that this structural evolution is closely related to the dynamic behavior of lithium vacancies within the material. Specifically, during the charging process, extensive extraction of lithium ions leads to the formation of a significant number of lithium vacancies, rendering the cathode material thermodynamically unstable. This effect is particularly pronounced under high cutoff voltage conditions, where deeper delithiation further promotes vacancy formation. Such structural changes have two major consequences: (1) The accumulation of lithium vacancies substantially slows down the lithiation kinetics during the subsequent discharge process, leading to increased overpotential at the end of the discharge half-cycle. This manifests as a sharp voltage drop and rapid capacity fade. (2) When kinetic conditions permit, the cathode material undergoes structural reconstruction to eliminate these vacancies. This vacancy-healing process is supported by the gradual capacity recovery observed in Figure 5d and Figure S39 (*ACS Energy Letters 2019, 4 (8), 1902–1906*).

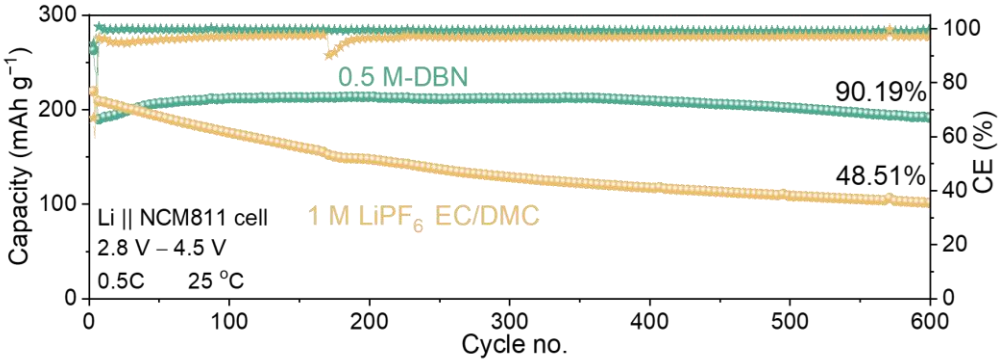

Figure 5d. Cycling performance of Li||NCM811 cell at 0.5C, 4.5 V.

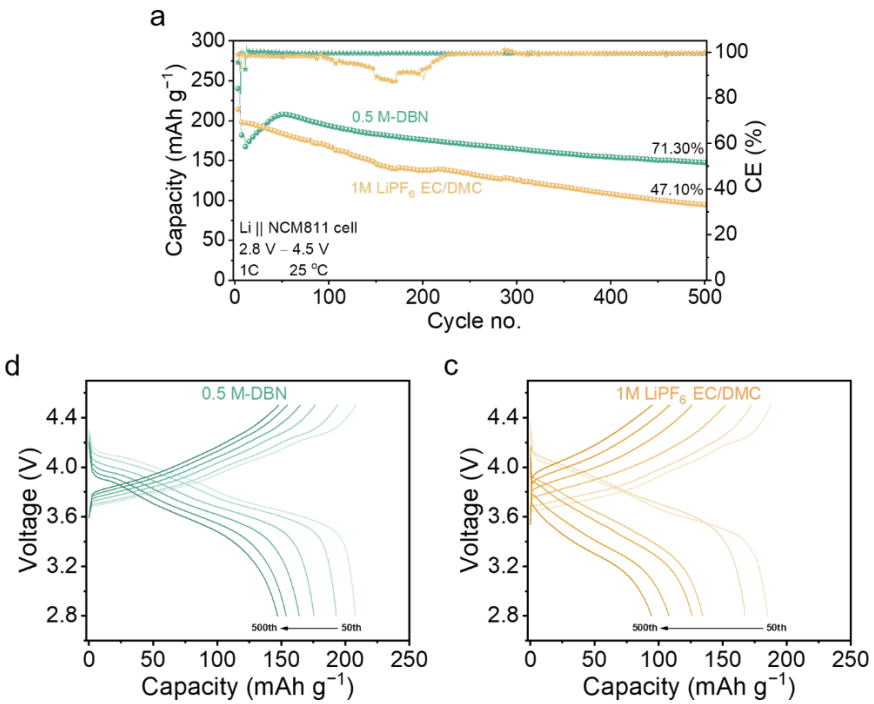

Figure S39. (a) Cycling performance and CE of NCM 811 cathode in 0.5 M-DBN and 1 M $LiPF_6$ EC/DMC electrolytes at 1 C multiplicity with up to 4.5 V. Corresponding voltage profiles of NCM811 cathode in 0.5 M-DBN (b) and 1 M $LiPF_6$ EC/DMC (c) electrolytes.

11. In Figure 5l "D_{Li+} of NCM523 cathode" should be "D_{Li+} of NCM811 cathode"?

Response: We thank the reviewer for the careful review of our manuscript. In

accordance with the reviewer's suggestion, we have corrected "NCM523" to "NCM811" in the caption of Figure 5i. The corresponding statement in the manuscript text (line 213) has also been revised accordingly: *"(k) The GITT technique was used to measure the charge/discharge voltage profiles and (l) corresponding D_{Li+} of NCM811 cathode after 100 cycles with different electrolytes."*

12. The author claims that the GED of the pouch cell is 452.47 Wh/kg, the battery design in detail needs to be clarified.

Response: We sincerely thank the reviewer for the rigorous and constructive evaluation of our work. We apologize for the oversight during manuscript proofreading, in which the weight of the aluminum-laminated pouch was inadvertently excluded from the energy density calculation of the pouch cell. We have now re-evaluated the relevant data, and the corrected value (as presented in Supplementary Table S5) shows that the system still achieves a high energy density of 430.51 Wh kg^{-1}, with the total mass of the aluminum pouch included. This corrected result continues to demonstrate a significant advantage over other reported non-flammable electrolyte systems (see comparative data in Fig. 6c), thereby reinforcing the innovative value of our work in simultaneously enhancing both energy density and safety.

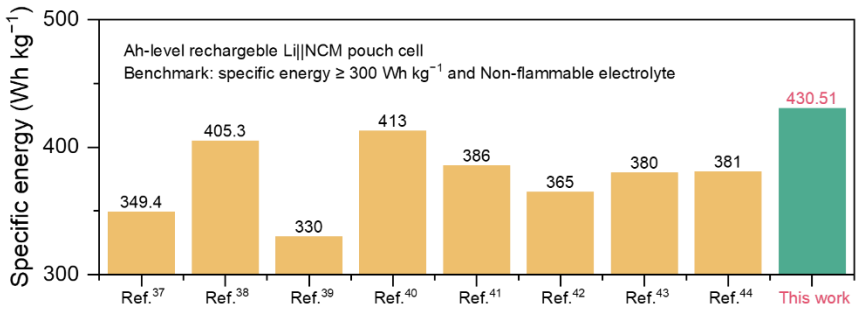

Figure 5c. In both published literature and this work, lithium metal pouch cells with high energy density and non-flammable electrolytes exhibit state-of-the-art performance.

Table S5. Pouch cell energy density calculation

	Parameter	Value
Cathode (NCM811 with Al current collector)	Discharge Capacity	221 mAh g^{-1}
	Area weight	22 mg cm^{-2}
	Active material ratio	97%
	Area capacity	4.86 mAh cm^{-2}
	Number of layers	8
	Weight	15.13 g
Li anode	Li thickness	50 μm
	Number of layers	9
	Weight	1.92 g
Collector (Cu)	Cu thickness	8 μm
	Weight	1.93 g
Electrolyte	E/C ratio	1.75 g Ah^{-1}
	Weight	5.25
Separator	type	Polyethylene
	Weight	0.5 g
Package and tabs	Weight	1.75 g
	Size	7 cm*10 cm
Pouch cell	Discharge capacity	3 Ah

	Average voltage	3.8 V
	Weight	26.48 g
	Energy density	430.51 Wh kg^{-1}

Specific energy = discharge energy (Wh) / total weight (kg). This is a more precise calculation method compared to the method: Specific energy=discharge capacity (Ah) × mid-value voltage (V) / total weight (kg).

13. TEP based electrolyte could be retardant at a content of 5-10% wt. The molecule itself has a high reactivity with lithium metal, which has been reflected in the optimized coulombic efficiency of only 97.5%. This coulombic efficiency makes it difficult for practical applications in lithium metal cells. Does the author compare TEP to other retardant solvents?

Response: Thank you for the reviewer's thorough evaluation and valuable comments on our work. In response to your concern, we would like to clarify the following: although the addition of 5–10% TEP can significantly enhance the flame retardancy of the electrolyte, the presence of 90–95% flammable solvents still poses potential safety risks. To address the reactivity between TEP and lithium metal, we introduced lithium salts with low LUMO energy levels, which preferentially decompose to form a stable anion-derived interphase. This interphase effectively prevents direct contact between TEP and lithium metal. While there remains room for further improvement in Coulombic efficiency, the achieved performance is already at an advanced level compared to previously reported phosphate ester-rich electrolyte systems (Sustainable Energy Fuels, 2022, 6, 1281–1288; ACS Energy Lett. 2025, 10, 4, 1700–1711).

In addition, we conducted a systematic experimental study to compare the performance of different flame retardants. Three commonly used flame retardants (TMP, TEP, and PFPN) were individually added to a commercial electrolyte (1 M $LiPF_6$ in EC/DMC, denoted as S) in volumes of 50 μL and 100 μL. Their Coulombic efficiencies (CE) were evaluated using the Aurbach method. The results showed that the S + 100 μL TEP system exhibited the highest CE among the flame-retardant-modified electrolytes, reaching 94.63%, which is an improvement over the baseline commercial electrolyte (88.34%) (Figure caption4a). However, this value still falls short of the CE achieved by the 0.5 M-DBN electrolyte (99.18%) (Figure caption4b). The superior performance of the 0.5 M-DBN system is primarily attributed to the synergistic decomposition of the three lithium salts, which forms a highly stable triphasic interphase with enhanced interfacial stability and Li^+ transport properties. Please refer to the description in lines 223–226 of the manuscript: "*Furthermore, the incorporation of alternative flame-retardant additives into the 1 M $LiPF_6$ EC/DMC electrolyte resulted in markedly lower Coulombic efficiency compared to the 0.5 M DBN-based system, thereby reinforcing the effectiveness of the proposed approach (Figure S27).*"

Therefore, this fully flame-retardant electrolyte system—composed of pure TEP as the solvent and three lithium salts as solutes—features a uniquely structured interfacial layer that not only mitigates the corrosive effects of the flame retardant on the lithium metal anode but also enables high Coulombic efficiency.

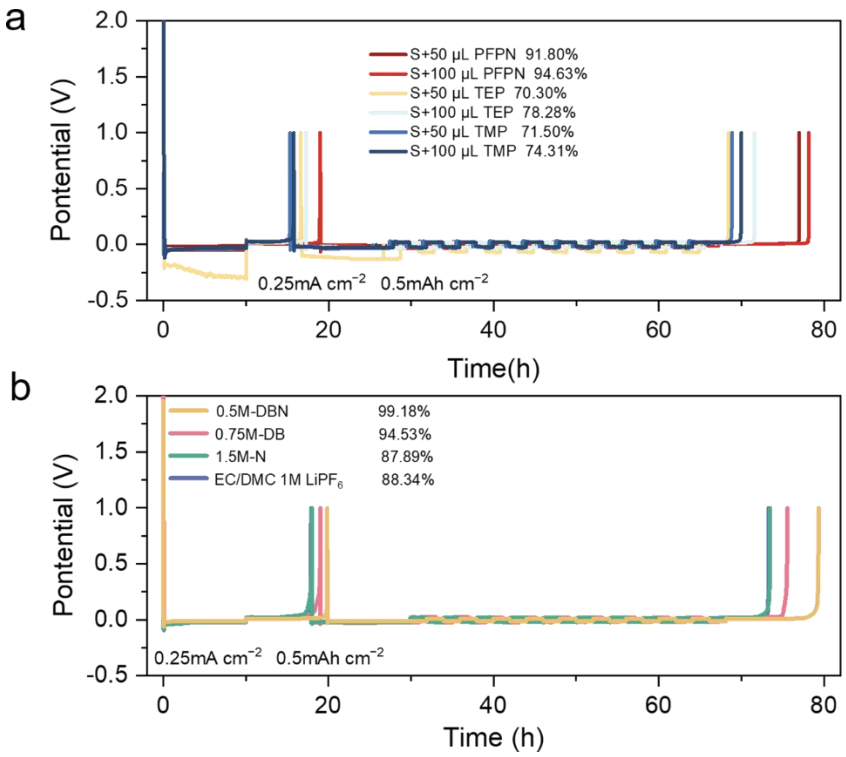

Figure caption4. (a) Coulombic efficiencies (CE) of commercial electrolytes containing TMP, TEP, and PFPN additives measured by the Aurbach method. (b) Coulombic efficiency was determined by a modified Aurbach method at 25 °C and 0.25 mA cm^{-2} current density.

14. Fig "S33" in line 327 should actually be Fig S37. Please confirm.

Response: We thank the reviewer for the careful review of our manuscript. The reference to "Fig. S33" in the main text (line 327) has been corrected to "Fig. S37." In addition, the corresponding description at line 213 has been revised accordingly: *"Figure S37 displays the F1s spectra, which also confirms that the LiF content on the cathode surface of battery with 0.5 M-DBN electrolyte is higher than that of with the commercial electrolyte. This verified the formation of inorganic-rich CEIs."*

Reviewer 3

This manuscript reports a non-flammable phosphate-based electrolyte for lithium metal batteries using a ternary-salt combination of LiDFOB, LiNO3, and LiBF4 in triethyl phosphate (TEP). The electrolyte facilitates the formation of a solid electrolyte interphase (SEI) enriched with B-O and Li3N in the inner layer and LiF in the outer layer, contributing to improved stability and reversibility of the lithium metal anode. While the study presents comprehensive characterization, its novelty does not appear to lie in new material design or good performance. A similar electrolyte formulation of 1 M LiDFOB together with 0.2 M LiNO3 dissolved in TEP, ethylene carbonate (EC) and dimethyl carbonate (DMC), with better Li metal stability (Coulombic efficiency of ~98% vs. 97.2% in this work), has been reported several years ago in the Journal of Electrochemical Society (J. Electrochem. Soc., 166, A2523). Moreover, some other phosphate electrolytes in literatures have also shown comparable and higher CE with non-flammable feature (e.g., Batteries & Supercaps, 2023, 6, e202200453; Batteries & Supercaps, 5, e202100407; Energy Storage Materials, 2024, 71, 103603; ACS Nano 2023, 17, 23, 24227–24241). However, this work may potentially provide some insights in the mechanistic understanding, if some unclear points can be clarified.

Response: We sincerely thank the reviewer for the thoughtful evaluation and valuable suggestions regarding our work. With respect to the research field of stabilizing TEP-based electrolytes through lithium salt regulation, we believe that our study differs significantly from the references cited by the reviewer. A comparative analysis between our system and the five referenced works *(J. Electrochem. Soc., 166, A2523; Batteries & Supercaps 2023, 6, e202200453; Batteries & Supercaps 2023, 5, e202100407; Energy Storage Materials 2024, 71, 103603; ACS Nano 2023, 17, 23, 24227–24241)* is provided below to highlight the distinctiveness and innovation of our approach:

We note that Reference 1 *(J. Electrochem. Soc., 166, A2523)* has two key limitations: (1) The employed TEP/EC/DMC co-solvent system (8.4:8.4:83.2 v/v) remains carbonate-dominated (91.6% by volume), which cannot ensure full non-flammability of the electrolyte. (2) The study only tested the electrolyte with an LFP cathode (2.0–4.0 V), without verifying compatibility with high-voltage, high-nickel cathodes. In contrast, our work achieves three major breakthroughs: (1) Development of a fully non-flammable, TEP-based electrolyte system without carbonate solvents; (2) Successful compatibility with NCM811 cathodes over a wide voltage window (2.8–4.6 V); (3) A novel voltage-driven anion migration mechanism enabling the formation of a gradient interfacial layer. It is particularly worth noting that the interfacial stabilization in Reference 1 relies mainly on the preferential reduction of $LiNO_3$, whereas our study establishes a fundamentally distinct theoretical framework based on anion migration and selective enrichment under electric fields.

Reference 2 *(Batteries & Supercaps 2023, 6, e202200453)* employed a TEP/$LiNO_3$/FEC ternary system, where the electrode–electrolyte interface was regulated through the synergistic decomposition of FEC and $LiNO_3$ additives. Although both this study and ours focus on interfacial engineering, the underlying regulation strategies differ fundamentally. Specifically, Reference 2 relies on a static, additive-assisted approach, where interfacial layers are chemically formed through the introduction of functional additives. In contrast, our work introduces a novel voltage-driven dynamic interfacial construction mechanism, wherein anions undergo in situ electrochemical migration and gradient decomposition under an electric field, leading to the spontaneous formation of a structured interphase. This dynamic, electrochemically-driven strategy stands in sharp contrast to the static, additive-based method adopted in Reference 2, underscoring the originality and advancement of our proposed interfacial design concept.

Reference 3 *(Batteries & Supercaps 2023, 5, e202100407)* reported a high-dilution electrolyte system by combining TEP with fluorobenzene (FB) as a diluent and using LiFSI as the lithium salt. In this work, TEP serves as the primary solvent, while FB is introduced to mitigate the high viscosity and low ionic conductivity typically associated with highly concentrated electrolytes. The study focuses on solvation structure regulation, aiming to form an anion-dominated solvation sheath and enhance interfacial stability through solvent–salt interactions. In contrast, our study employs a binding energy–driven strategy involving the synergistic use of LiODFB, $LiBF_4$, and $LiNO_3$. By leveraging the differences in binding energies between Li^+ and various anions, we achieve selective interfacial enrichment and controlled SEI composition. Therefore, the core mechanism and scientific rationale of Reference 3 are fundamentally different from ours.

Reference 4 *(Energy Storage Materials 2024, 71, 103603)* proposed a TEP-based electrolyte system incorporating a ternary lithium salt combination of LiTFSI, LiDFOB, and $LiNO_3$. While both this study and ours utilize multi-salt strategies to stabilize phosphate-based electrolytes, the underlying mechanisms differ fundamentally. Reference 4 stabilizes the electrode–electrolyte interface primarily through the synergistic effect of decomposition products derived from the three lithium salts. In contrast, our work for the first time uncovers the differentiated electrochemical migration behavior of $DFOB^-$, NO_3^-, and BF_4^- anions under an applied electric field. This selective migration leads to spatially controlled reduction, resulting in the formation of a gradient SEI structure composed of a B–O/Li_3N-rich inner layer and a LiF-rich outer layer. Therefore, the core principles and mechanistic foundations of Reference 4 are fundamentally different from those of our study.

Reference 5 *(ACS Nano 2023, 17, 23, 24227–24241)* achieved a synergistic regulation of the 1.5 M LiTFSI/TEP electrolyte by incorporating dual additives, $LiNO_3$ and dimethoxyethane (DME). This approach led to the formation of a thin, dense, and robust electrode/electrolyte interface on both the lithium anode and high-nickel cathode surfaces, enhancing the compatibility between the electrodes and electrolyte. Unlike our study, which focuses on synergistic regulation of lithium salts to optimize the interfacial composition, this work relies on the cooperative addition of solvents and lithium salts to enable high-voltage lithium-metal batteries. Therefore, Reference 5 and our study differ fundamentally in their approach and underlying mechanisms.

1. The key finding of this work is the contrasting response of $DFOB^-$/NO_3^- anions vs. BF_4^- anion under electric field, where the former migrate towards Li metal anode while the latter move away, as evidenced by molecular dynamic (MD) simulations. This phenomenon is thought to drive the preferential reduction of $DFOB^-$ and NO_3^- anions to form an SEI with B-O and Li_3N-rich inner layer and LiF-rich outer layer.

If this phenomenon truly occurs in lithium metal batteries, it would be interesting. However, there are several unclear points. The first is concerning the model of MD calculations. Does it consider the effect of electric double layer in the calculation? If not, the electric double layer itself has a species distribution, which might violate the calculation results in the paper, i.e., $DFOB^-$, NO_3^- and BF_4^- anions do not move in behaviors predicted by the MD simulation results. Second, since the Li^+ ion is coordinated with $DFOB^-$, NO_3^- or BF_4^- anion to form the charge-neutral ion pair, why can the anions in the ion pair move towards the Li metal anode under electric field? Third, what's the meaning of y axis in Figure 1c-1f? Does it reflect the real content of anions and solvents close to Li(100)? If it is, then why all anions and solvents just sum up to ~10%? Fourth, what's the rational of choosing Li(100) for calculation rather than

Li(110), the thermodynamically most stable plane, or other Li planes? The fifth point, the statistcal distribution of $DFOB^-$, NO_3^- and BF_4^- does not differ too much in Figure 1c-1f, ~1.0 for the former peak and 0.8 for the BF_4^- peak. It is not a significant difference for the amount of $DFOB^-$, NO_3^- and BF_4^- on Li surface.

Response: We sincerely thank the reviewer for the thorough and careful evaluation of our manuscript. The reviewer has raised five critical questions, which we address in detail below.

In our calculations, the presence of the electric double layer was fully considered. The electrochemical double layer refers to a nanoscale structure formed by charge separation at the electrode/electrolyte interface, comprising the charge distribution on the electrode surface and the counterion arrangement in the electrolyte. By introducing an external electric field in the simulations, the anode interface attracts Li^+ ions under the influence of the field, leading to a specific ion aggregation near the anode. This behavior can, to a certain extent, be regarded as representing the formation of an electric double layer.

Second, even though Li^+ forms electrically neutral ion pairs with $DFOB^-$, NO_3^-, or BF_4^-, the anions can still move toward the lithium metal anode under an applied electric field. This phenomenon arises because Li^+ ions must reach the anode to accept electrons and be deposited. When the binding between Li^+ and the anion is strong, the anion is partially dragged along by the migrating Li^+, resulting in its transport toward the anode (*Energy Storage Materials,2022,45,1-13*).

Regarding the third question, we sincerely apologize for the oversight in labeling the y-axis. After careful verification, we confirm that the y-axis in Figures 1c–1f and Figure S13 should represent the number density, with the correct label being “Number density (N nm^{-3}).” This parameter reflects the number of particles per unit volume and is

therefore capable of accurately indicating the local content of anions and solvent molecules near the Li(100) surface. It is also important to note that, as number density is a particle-based quantity, the individual component curves (anions, solvents, etc.) are plotted independently. Thus, the sum of their values at each position does not necessarily equal a meaningful or fixed total percentage.

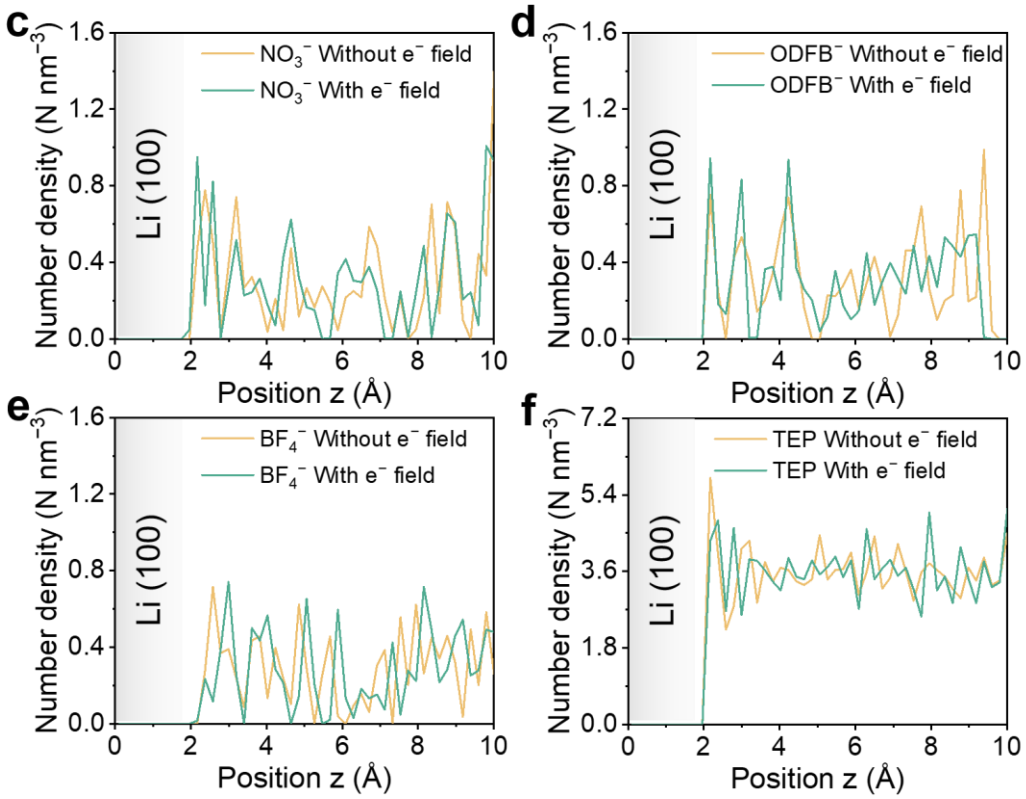

Figure 1c-f. Quantity distribution in the z-direction for each substance. (c)NO_3^-, (d)ODFB$^-$, (e)BF_4^- and (f)TEP.

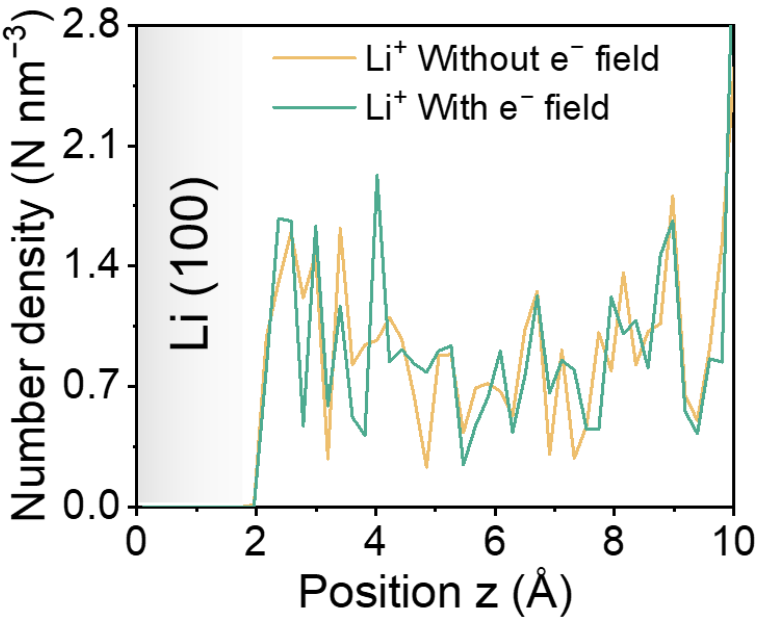

Figure S13. Number distribution of lithium ions in the Z-direction with and without an electric field.

Regarding the fourth point, we appreciate the reviewer's valuable suggestion. It is indeed well established that the Li(110) surface is the most thermodynamically stable facet and plays a significant role in promoting uniform lithium deposition. However, we would like to clarify that the molecular dynamics simulations in this study focus primarily on the migration behavior of anions in the electrolyte under an applied electric field, rather than on the lithium deposition process itself. Due to this difference in research objectives, the impact of surface orientation on our conclusions is relatively limited. It is also worth noting that the use of the Li(100) surface in molecular dynamics simulations of lithium metal interfaces has precedent in the literature (e.g., *Energy Storage Materials*, 2022, 45, 1–13). Our choice of surface is thus consistent with prior studies, further supporting the validity of our modeling approach.

Regarding the fifth question, we acknowledge the minor differences in the statistical distributions of $DFOB^-$, NO_3^-, and BF_4^- in Figure 1c-1f, where the peak value for $DFOB^-$ is 1.0, and for BF_4^- is 0.8 N nm^{-3}. At the Li surface, there is no significant difference in the quantities of $DFOB^-$, NO_3^-, and BF_4^-. However, it is important to note that our calculations were conducted in a relatively small molecular box. While the peak difference is only 0.2 N nm^{-3}, if this were extended to the actual electrode-electrolyte interface, the number of these species would show a substantial difference.

2. For the in-situ FTIR test which can potentially validate the MD simulation results, there are also many confusing issues. The manuscript writes that "during plating, …Notably, the reversibility of BF_4^- is significantly higher compared to that of $ODFB^-$, indicating that $ODFB^-$ is more extensively consumed". This phenomenon is difficult to interpret, since the electrode polarization should be negative for the plating process in Li/Cu cell, which will expel the negatively charged anions from Li metal surface instead of increasing their concentration. On the other point of view, the decrease in $DFPB^-$ intensity might be attributed to the negative electric field rather than the consumption of $DFPB^-$.

A more fatal defect of the FTIR result is the strong intensity of BF_4^- on the Li surface, which is completely contradictory to the MD results in Figure 1 which claims that BF_4^- can hardly approach the Li metal and thus weakens its reduction. The discrepancy between the FTIR observation and the MD simulation highlights a significant gap in the study's coherence.

Response: We sincerely thank the reviewer for their in-depth evaluation and constructive comments. In response to the concern regarding the accuracy of peak assignment and the interpretation of the reaction mechanism, we have thoroughly re-

examined our experimental data and refined the corresponding analyses. The core revisions are detailed as follows:

After recalibrating the in-situ infrared spectroscopy data, we have corrected the peak assignments: the peak at 833.24 cm^{-1} corresponds to the characteristic vibration of LiF; the peaks at 958.62 cm^{-1} and 977.90 cm^{-1} are attributed to free TEP and coordinated TEP (P–O–C stretching vibration), respectively; the peak at 1026.13 cm^{-1} is ascribed to coordinated LiODFB (Li^+–$ODFB^-$ complex, denoted as coor ODFB); and the 1253.73 cm^{-1} peak arises from the symmetric stretching vibration of the P=O bond in TEP. It is important to note that the in-situ FTIR measurements were performed in transmission mode, where the direction of spectral peaks correlates with changes in species concentration: downward peaks indicate an increase in content, while upward peaks reflect consumption.

In the Li||Cu half-cell system, the first stage (0–120 min) corresponds to Li^+ stripping from the lithium metal anode and its insertion into the copper current collector, while the second stage (120–240 min) involves the oxidation of metallic Li on the copper mesh ($Li \rightarrow Li^+ + e^-$) followed by Li^+ migration and deposition onto the lithium side. Spectral analysis shows a continuous decrease in the intensity of the coordinated TEP peak (977.90 cm^{-1}), accompanied by an enhancement of the free TEP signal (958.62 cm^{-1}), directly evidencing Li^+ desolvation at the electrode interface, with dissociation of the TEP coordination structure and release of free molecules.

Notably, the consumption peak of coordinated LiODFB (1026.13 cm^{-1}) retains 72.62% of its final delithiation intensity by the end of the stripping phase. If, as the reviewer suggested, the disappearance of the coor $ODFB^-$ signal were merely caused by electrostatic repulsion after desolvation, a recovery (i.e., weakening of the consumption peak) should be observed during the stripping stage. However, this contradicts the experimental results. Therefore, we propose that the irreversible consumption of LiODFB is more plausibly attributed to electron transfer reactions of $ODFB^-$ anions at highly reductive potentials ($ODFB^- + e^- \rightarrow$ decomposition products), which

subsequently participate in the formation of anion-derived solid electrolyte interphase (SEI).

For comparison, we also investigated the conventional 1 M $LiPF_6$/EC–DMC electrolyte system. The results indicate that $LiPF_6$-coordinated peaks exhibit highly reversible behavior throughout cycling (reversibility >92%), in sharp contrast to the LiODFB system. This confirms that strongly coordinating anions (e.g., $ODFB^-$) tend to undergo irreversible decomposition and contribute to SEI formation.

We have revised and improved the textual descriptions according to the reviewer's comments, as detailed below: "As shown in Figure 2a and Figure S17, during the lithium deposition stage (i.e., the desolvation process), the pronounced consumption peak at 977.90 cm^{-1} corresponds to the gradual depletion of solvated TEP, while the emerging peak at 958.62 cm^{-1} indicates the release of desolvated solvent molecules at the electrode interface[14]. Figure S16 presents the in situ infrared spectra of the 1 M $LiPF_6$ EC/DMC electrolyte system. Furthermore, by comparing the ratio of characteristic peak areas at the end of lithium deposition and during the stripping stage, we quantitatively analyzed the interfacial behavior of surface anions. Notably, PF_6^- (which weakly coordinates with Li^+) exhibits significantly higher reversibility than $ODFB^-$, indicating that $ODFB^-$ is more extensively consumed in interfacial reactions (Figure 2b). This observation aligns well with the theoretical calculations, suggesting that $ODFB^-$ preferentially decomposes and contributes to the formation of the inner interfacial layer. More interestingly, an enhanced peak at 833 cm^{-1} associated with LiF was observed, further confirming the formation of an inorganic-rich interphase (Figure S17)[25]."

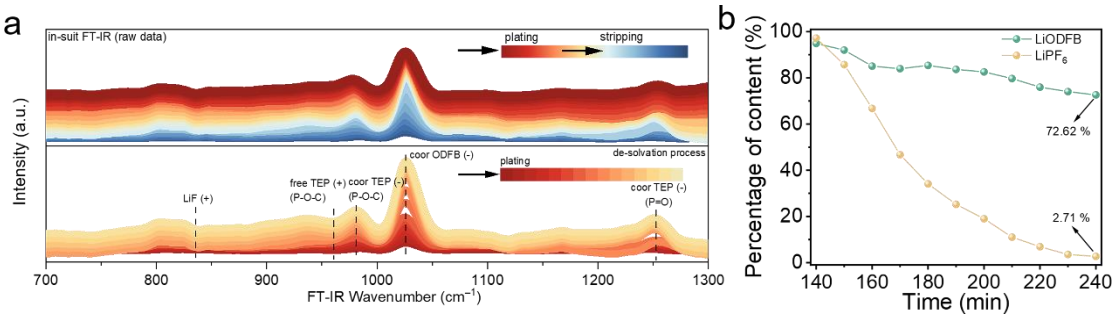

Figure 2a-b. Contour plots of In-suit Fourier-transform Infrared (FTIR) spectra of the electrode/electrolyte interfaces in a 0.5 M-DBN electrolyte (a) and their content variations (b).

Also, the LiF and free TEP peaks are almost not visible, whose change cannot be discerned during test. This is problematic because these peaks are expected to be critical indicators of the formation and evolution of the SEI, and their absence raises doubts about the accuracy of the in-situ FTIR analysis or the interpretation of the spectra.

Response: We sincerely thank the reviewer for the careful evaluation and valuable suggestions regarding our work. In response to the concern about the visibility of the IR characteristic peaks for LiF and free TEP, we have conducted a detailed re-examination. Our analysis reveals that the original spectra had relatively broad line widths, which led to insufficient resolution at the key positions of 833.24 cm^{-1} (LiF) and 958.62 cm^{-1} (free TEP). To more clearly present these two characteristic peaks, we compared the FTIR spectra at two representative time points: 0 min (initial state) and 240 min (final state) (Figure caption5). The absorption signals at the aforementioned wavenumbers are clearly observable in this comparison, confirming the presence of LiF and free TEP.

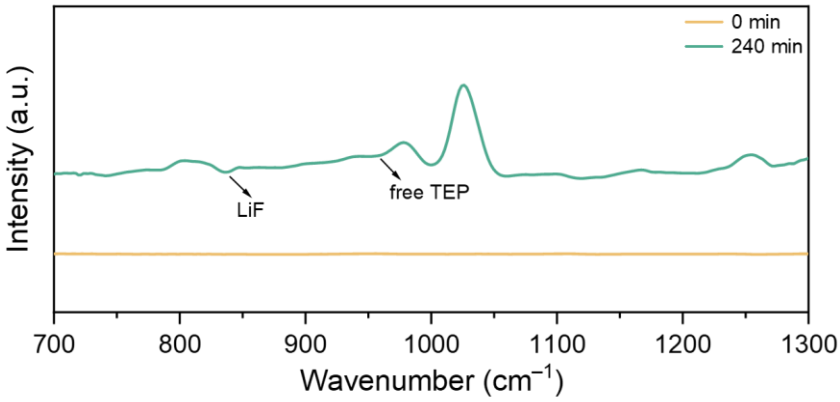

Figure caption5. In-situ infrared spectra at 0 min and 240 min.

3. The formation mechanism of dual-layered SEI is not clear.

Since $DFOB^-$ can be decomposed to form B-O species in the inner SEI, why can't we detect large amount of LiF in the inner layer, given that $DFOB^-$ can donate element F during decomposition?

Response: We sincerely thank the reviewer for their thorough evaluation of our manuscript. The central mechanism of our work lies in the differences in binding energies between lithium ions (Li^+) and various anions ($ODFB^-$, NO_3^-, and BF_4^-). Specifically, Li^+ exhibits significantly stronger binding with $ODFB^-$ and NO_3^- compared to BF_4^-. Under an applied electric field, Li^+ preferentially co-migrates with the more strongly bound $ODFB^-$ and NO_3^- anions, leading to their enrichment near the lithium metal surface, while BF_4^-, due to its weaker interaction with Li^+, tends to be excluded from the interface. This dynamic ion distribution ultimately results in the formation of a gradient-structured SEI layer, characterized by a B–O bond- and Li_3N-rich inner region and an LiF-dominated outer region.

We further appreciate the reviewer's insightful comment regarding the predominance of B–O species rather than LiF in the inner SEI layer derived from the decomposition

of the $ODFB^-$ anion. This observation can be attributed to the relatively low bond dissociation energy of the B–O bond in the $DFOB^-$ anion (210.7 kJ mol^{-1}), which decreases further to −50.1 kJ mol^{-1} in the DFOB• radical state (*Nature Energy* 2018, 3, 739–746). The significantly weakened B–O bond makes it more susceptible to electrochemical cleavage during interfacial reactions, thereby favoring the formation of B–O-rich species in the inner SEI. Consequently, the SEI is dominated by $ODFB^-$-derived B–O components rather than LiF in its inner region. This mechanism is in excellent agreement with previously reported decomposition pathways of the $DFOB^-$ anion (*Nature Energy* 2018, 3, 739–746).

4. What's the role BF_4^- plays in this electrolyte? From the paper, it seems that the binary combination of $DFOB^-$ and NO_3^- can have a positive effect on the Li metal anode.

Response: We sincerely thank the reviewer for the careful evaluation of our work. In our electrolyte design, the BF_4^- anion—owing to its relatively weak interaction with Li^+ (ionic radius: 0.227 nm)—serves a dual function: it facilitates the formation of a LiF-rich outer SEI layer, while its high degree of dissociation significantly enhances the ionic conductivity of the electrolyte. It is worth emphasizing that although the NO_3^-/$ODFB^-$ binary system can effectively stabilize the lithium metal interface, it also leads to increased viscosity (up to 13.4 cP in the 0.75 M-DN system) and reduced ionic conductivity (3.68 mS cm^{-1}). In contrast, the introduction of $LiBF_4$ in the 0.5 M-DBN system enables a synergistic effect through ion coordination, which not only maintains interfacial stability but also improves the ionic conductivity to 5.13 mS cm^{-1} (an increase of 39%) and reduces viscosity to 9.44 cP (a 30% decrease) (Figure caption6). These results clearly demonstrate the dual enhancement role of $LiBF_4$ in both interfacial modification and electrolyte physicochemical optimization.

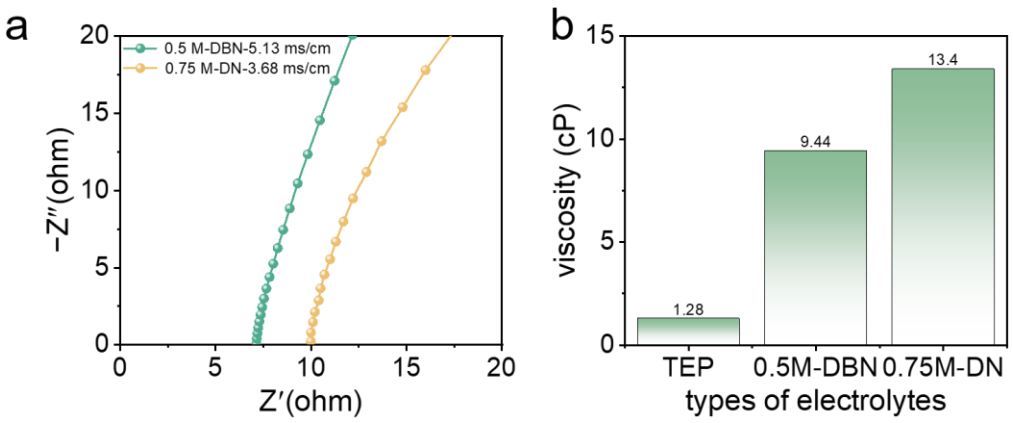

Figure caption6. (a) The ionic conductivity of the 0.5 M-DBN and 0.75 M-DN electrolytes. (b) The viscosity of TEP, 0.5 M-DBN, and 0.75 M-DN electrolytes

5. The reported Coulombic efficiency values of Li/Li symmetic cells are very confusing and potentially misleading. The manuscript states that "the Li||Li symmetric battery assembled with 0.5 M-DBN electrolyte demonstrated a higher CE of 99.18% after 10 cycles at a current density of 0.25 mA cm^{-2} and with an area capacity of 0.5 mAh cm^{-2} than the Li||lithium symmetric batteries assembled with 0.75 M-DB (94.53%), 1.5 M-N (87.89%), and 1M $LiPF_6$ EC/DMC (88.34%) electrolytes".

However, since Li reserivor is super excesive in the Li/Li cell, how can the authors calculate the CE? This expression may not be considered professional or appropriate in a Li metal battery study.

Response: We sincerely thank the reviewer for the insightful comments. The reviewer's concern regarding the reported Coulombic efficiency (CE) is entirely reasonable. We deeply apologize for the mistake in our original manuscript, where the "Li||Cu cell" was incorrectly described as a "Li||Li cell." This has now been corrected.

To clarify, the CE measurements in our study were performed using Li||Cu half-cells to evaluate the reversibility of lithium plating/stripping in the investigated electrolyte system. Specifically, we adopted the Aurbach method *(Adv. Energy Mater. 2018, 8,1702097, Electrochimica Acta 1997, 42, 697-718)*, which enables a more accurate assessment of electrolyte reversibility. Initially, lithium was deposited at a current density of 0.25 mA cm^{-2} until a predetermined capacity (Q_t) was reached, forming a lithium reservoir on the copper substrate. This was followed by n galvanostatic plating/stripping cycles (n = 10 in our case) using a current density of 0.25 mA cm^{-2} and a fixed capacity of 0.5 mAh cm^{-2} per cycle. The remaining lithium was subsequently stripped at 0.25 mA cm^{-2} up to 1 V to determine the residual capacity (Q_s). The average Coulombic efficiency (CE_{avg-n}) was then calculated using the following equation:

$$CE_{avg-n} = \frac{nQ_C + Q_s}{nQ_C + Q_t}$$

Where Q_c is the plating/stripping capacity for each of the n cycles (fixed at 0.5 mAh cm^{-2}), Q_t is the initial lithium reservoir capacity, and Q_s is the final stripped capacity from the copper substrate.

We have revised the relevant statements in the manuscript according to the reviewer's suggestions. The detailed modifications can be found in Lines 214–219 of the revised manuscript: *"In addition, the Li||Cu symmetric battery assembled with 0.5 M-DBN electrolyte demonstrated a higher CE of 99.18% after 10 cycles at a current density of 0.25 mA cm^{-2} and with an area capacity of 0.5 mAh cm^{-2} than the Li||Cu symmetric batteries assembled with 0.75 M-DB (94.53%), 1.5 M-N (87.89%), and 1M $LiPF_6$ EC/DMC (88.34%) electrolytes (Figure S27), which further emphasizes the benefits of the three-phase SEI formation."*

6. The cathode degradation comparsion with XRD characterizations (Figure 4c-4e) does not perform in the perfectly same condition for the reported electrolyte and base electrolyte. The $LiPF_6$ EC/DMC electrolyte has a higher ionic conductivity, thus enabling higher initial discharge capacity for Li/NMC811 cell. This corresponds to higher utilization rate of Li in the NMC811 cathode under the same cut-off voltage. Since it is widely accepted that the degradation of high-Ni cathode is closely linked to the Li de-intecalation ratio, the higher Li de-intecalation for cathode in the base LiPF6 EC/DMC electrolyte can leads to faster cathode degradation.

Response: We sincerely thank the reviewer for the valuable comments. Regarding the comparison of in situ XRD data, we have unified all charge–discharge curves to the same vertical scale for better consistency, as shown in Figure 4c. Additionally, the phase transition angles of the NCM811 cathode are clearly labeled in Figures 4d and 4e to facilitate a more direct comparison of structural evolution.

We fully agree that ionic conductivity can influence the initial discharge capacity. In addition, the initial capacity is also affected by other factors, such as the loss of active lithium caused by the formation of SEI/CEI and the oxidation stability of the electrolyte. Notably, although the charging time in the 0.5 M-DBN electrolyte is longer (7057 s vs. 6381 s for 1 M $LiPF_6$ EC/DMC), which theoretically should result in a higher degree of delithiation, the XRD peak shifts of the (003) and (101) planes in the NCM811 cathode are actually smaller when using the 0.5 M-DBN electrolyte (Figure caption 7). This result indicates that the NCM811 cathode cycled in the 0.5 M-DBN electrolyte undergoes a more reversible structural evolution and maintains structural integrity during cycling.

In summary, although the 0.5 M-DBN electrolyte delivers a higher discharge capacity, the superior CEI formed effectively suppresses structural phase transitions in NCM811, thereby enhancing its long-term cycling stability.

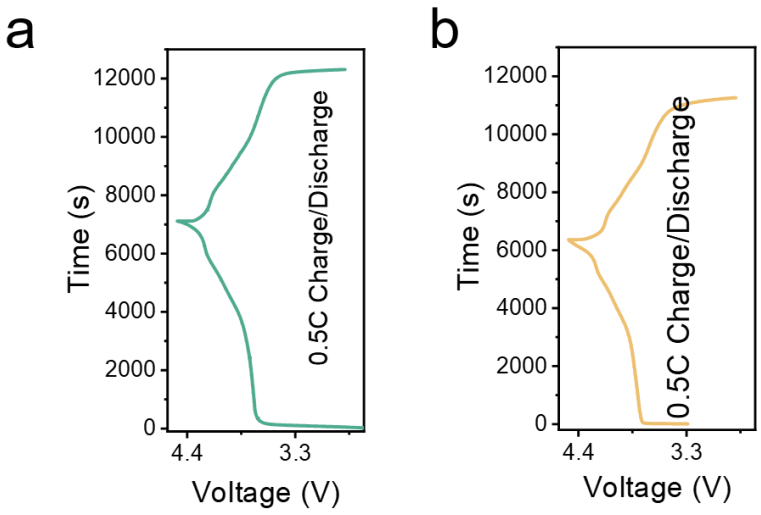

Figure caption 7. Charge–discharge curves of the NCM811 cathode using (a) 0.5 M DBN and (b) 1 M $LiPF_6$ EC/DMC electrolytes, plotted on the same Y-axis scale with charging and discharging times labeled.

7. The signal of Li_xC on the NMC811 cathode side is interesting. How can such a highly reducing material exist in the high voltage environment?

Response: We sincerely thank the reviewer for raising this critical and insightful point. In response to your comment, we have carefully re-examined the XPS spectra and the corresponding peak deconvolution procedures. Upon thorough evaluation, we acknowledge that the previously assigned Li_xC signal was likely the result of a misinterpretation during the C 1s peak fitting process. To address this, we adopted a more rigorous deconvolution strategy and reanalyzed the original data. The updated results no longer support the presence of a significant Li_xC phase on the surface of the NMC811 cathode.

We have accordingly revised the relevant figure and accompanying descriptions in the manuscript. The detailed modifications can be found in Lines [344–346] of the revised manuscript: *"We observed that in the 0.5 M-DBN electrolyte, the inner layer of the CEI exhibited a lower carbon content than the outer layer, in contrast to the commercial electrolyte, which showed the opposite trend (Fig. S36)."*

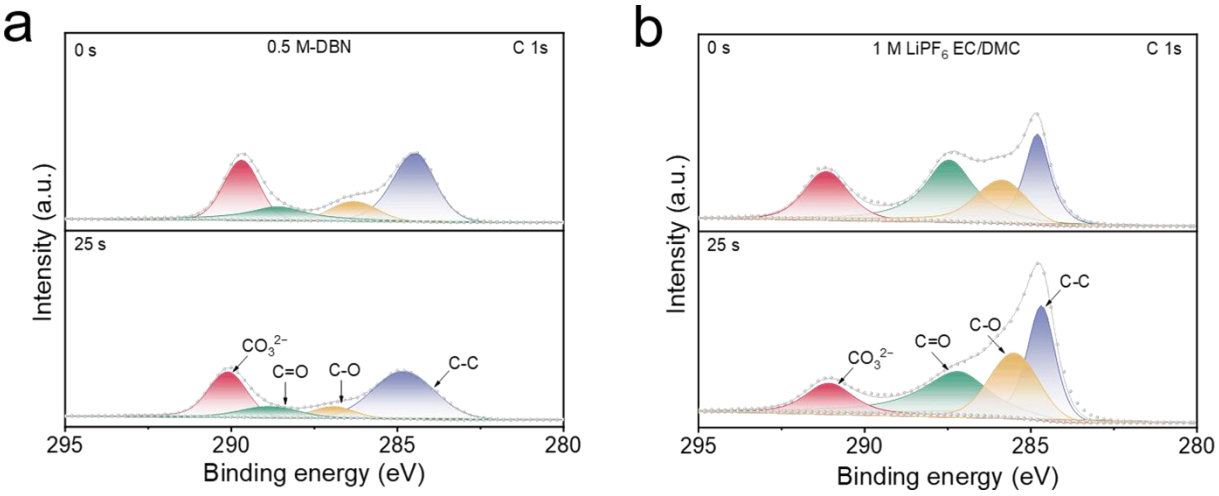

Figure S36. C1s XPS spectra of NCM811 cathode in 0.5 M-DBN (a) and 1 M $LiPF_6$ EC/DMC (b) electrolytes after different sputtering times (0 s, 25 s).

8. The calculation method of energy density of pouch cell is vague. Does it contain the weight of Al package? It is challenging to obtain such a high energy density with a relative high E/C ratio of 1.75 g/Ah. If the Al package weight was excluded, what's the real energy density for the cell?

Response: We sincerely thank the reviewer for the rigorous and constructive evaluation of our work. We apologize for the oversight during manuscript proofreading, in which the weight of the aluminum-laminated pouch was inadvertently excluded from the energy density calculation of the pouch cell. We have now re-evaluated the relevant

data, and the corrected value (as presented in Supplementary Table S5) shows that the system still achieves a high energy density of 430.51 Wh kg^{-2}, with the total mass of the aluminum pouch included. This corrected result continues to demonstrate a significant advantage over other reported non-flammable electrolyte systems (see comparative data in Fig. 6c), thereby reinforcing the innovative value of our work in simultaneously enhancing both energy density and safety.

Table S5. Pouch cell energy density calculation

	Parameter	Value
Cathode (NCM811 with Al current collector)	Discharge Capacity	221 mAh g^{-1}
	Area weight	22 mg cm^{-2}
	Active material ratio	97%
	Area capacity	4.86 mAh cm^{-2}
	Number of layers	8
	Weight	15.13 g
Li anode	Li thickness	50 μm
	Number of layers	9
	Weight	1.92 g
Collector (Cu)	Cu thickness	8 μm
	Weight	1.93 g
Electrolyte	E/C ratio	1.75 g Ah^{-1}
	Weight	5.25
Separator	type	Polyethylene
	Weight	0.5 g

Package and tabs	Weight	1.75 g
	Size	7 cm*10 cm
Pouch cell	Discharge capacity	3 Ah
	Average voltage	3.8 V
	Weight	26.48 g
	Energy density	430.51 Wh kg^{-1}

Specific energy = discharge energy (Wh) / total weight (kg). This is a more precise calculation method compared to the method: Specific energy=discharge capacity (Ah) × mid-value voltage (V) / total weight (kg).

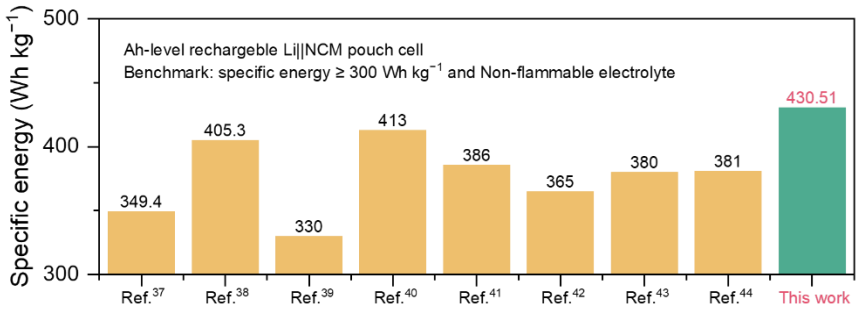

Figure 5c. In both published literature and this work, lithium metal pouch cells with high energy density and non-flammable electrolytes exhibit state-of-the-art performance.

Minor comments

1. Some other confusing points. For instance, “the height of layer deposited at the anode side is greater and the clump-like dendritic are larger when using the 0.5 M-DBN

electrolyte than that of battery with 1 M $LiPF_6$ EC/DMC electrolyte." This means that the Li metal is more porous in the reported electrolyte, which is not favorable.

Response: We sincerely thank the reviewer for the careful and insightful review of our manuscript. Due to our oversight, there was an inaccurate description regarding the phenomenon observed in the Scanning Probe Microscopy (SPM) analysis. We apologize for this mistake and have revised the relevant statements accordingly. The detailed modifications can be found in Lines 241–245 of the revised manuscript: *"As shown in Figure 3g–h and Figure S31, compared with the conventional 1 M $LiPF_6$ EC/DMC electrolyte system, the use of the 0.5 M-DBN electrolyte significantly reduces the thickness of the deposited layer on the lithium metal anode surface, while promoting a denser and bulk-like lithium deposition morphology. "*

"the leakage current density observed with the 1 M $LiPF_6$ EC/DMC electrolyte (10.17 mA cm-2)". mA level leakage current is so large, which can be larger than the current for cell test.

Response: We sincerely thank the reviewer for the careful reading and valuable comments. We would like to express our sincere apologies for the unit error in the manuscript, where "μA cm^{-2}" was mistakenly written as "mA cm^{-2}." This was indeed an oversight during proofreading. The error has now been corrected in the revised manuscript at line 278. The corrected statement reads as follows: *" In a rigorous float test at 4.6 V with an 8-hour retention time, the cell with the 0.5 M-DBN electrolyte had a leakage current density of 2.37 μA cm^{-2}, which was only 23% of the leakage current density observed with the 1 M $LiPF_6$ EC/DMC electrolyte (10.17 μA cm^{-2}) (Figure 4a). "*

2. "relatively complete and uniform CEI can … prevent unexpected electron transfer on the cathode/electrolyte interface". First, what's a complete SEI and unexpected

electron transfer? Second, why a complete CEI can prevent unexpected electron transfer?

Response: We sincerely thank the reviewer for the thorough evaluation of our work. Regarding the complete cathode–electrolyte interphase (CEI), its essential characteristics lie in the formation of a stable, uniform, and electrochemically/mechanically inert protective layer. The term "unexpected electron transfer" specifically refers to the phenomenon of electron tunneling. Although the electrolyte is intrinsically an ionic conductor, when the CEI contains structural defects (e.g., pores or cracks), electrons may tunnel from the cathode through the CEI into the electrolyte. This leads to undesirable oxidation reactions—such as the decomposition of EC solvent (EC → CO_2 + byproducts) *(Adv. Funct. Mater. 2023, 33, 2210465)*.

3. Some typo and grammar errors, e.g., “Successful decreasing the possibility of the parasitic reaction”

Response: We sincerely appreciate the reviewer’s professional evaluation and valuable suggestions. We have thoroughly revised the manuscript for grammar and language to ensure clarity, accuracy, and consistency in academic expression.

Thank you for your email informing us of your editorial decision on our manuscript (NCOMMS-25-16384A). According to the instructions in your email, we have carefully considered the helpful criticism from the referees and revised the manuscript accordingly. We provide a detailed response to the referees' criticism below. The changes made during revision are highlighted in yellow and the file is uploaded separately for review only.

Reviewer #1 (Remarks to the Author):

While the authors have addressed some initial concerns, critical issues remain unresolved, particularly regarding the mechanistic interpretation and its theoretical foundation. Without substantial revisions, the manuscript is not suitable for publication.

Response: Many thanks for the referee's valuable suggestion, especially, the insightful comments for further improving the quality of the manuscript. We have carefully addressed the issues as follows.

1. The use of the OPLS-AA force field for lithium metal, combined with a strong electric field of -1.0 V/nm, remains problematic. Although the authors cite precedent, they do not demonstrate that the observed ion migration trends persist under more realistic conditions. As the force field does not capture specific adsorption at the Li surface, the model likely exaggerates interfacial differences under the applied field. More seriously, despite the strong electric field, the anion distributions are noisy, and the field-induced effects cannot be clearly distinguished, raising serious concerns about the validity of the proposed mechanism. Furthermore, the SEI depth profiles, which the authors emphasize as key experimental evidence, reflect cumulative decomposition and transport processes over extended cycling and therefore do not directly validate the simulated initial anion distributions.

Response: We sincerely thank the reviewer for the thorough evaluation of our manuscript. Regarding the concern about employing the OPLS-AA force field to describe the interaction between lithium metal and lithium ions in lithium-metal-based systems, we have given this issue further consideration and performed additional validation calculations. Molecular dynamics (MD) simulations using the OPLS-AA force field in Gromacs confirmed that this force field indeed incorporates the interaction between lithium metal and lithium ions. Specifically, the extracted interaction energies were 320.56 kJ/mol (≈3.32 eV) under zero external electric field and 410.39 kJ/mol (≈4.25 eV) under an applied external electric field. To further validate the reliability of the OPLS-AA force field description, we conducted density functional theory (DFT) calculations of the adsorption energies of three lithium salts—$LiBF_4$, LiODFB, and $LiNO_3$—on lithium metal surfaces under electric field strengths of 0 V/nm, −0.1 V/nm, and −1 V/nm. Notably, under 0 V/nm and −1 V/nm (corresponding to the MD simulation conditions), the average adsorption energies of the three salts were 3.57 eV and 4.47 eV, respectively. These DFT results are in good agreement with the MD-derived interaction energies (3.32 eV and 4.25 eV), indicating that the OPLS-AA force field can reasonably capture the interaction between lithium metal and lithium ions to a certain extent. Moreover, the DFT results clearly reveal (**Figure S14-S15**) that the adsorption energies of LiODFB and $LiNO_3$ on lithium metal surfaces are significantly higher than that of $LiBF_4$. Therefore, within the system, LiODFB and $LiNO_3$ are more likely to be enriched at the lithium metal surface. Noted. In lines 112–113, the manuscript states: *"Meanwhile, the DFT calculations (Fig. S14-15) indicate that lithium metal exhibits a preferential adsorption toward $LiNO_3$ and LiODFB."*

Regarding the reviewer's concern about our use of the OPLS-AA force field, we note that OPLS-AA is able to reasonably describe the interactions between the Li metal anode and Li^+ ions. Specifically, in the absence of an applied electric field, the Li metal–Li^+ interaction energy predicted by this force field is approximately 320.56 kJ/mol (≈ 3.32 eV), which is very close to the average adsorption energy (3.57 eV) we obtained for the three lithium salts under the same conditions. Similarly, under an applied electric field, the interaction energy is about 418.39 kJ/mol (≈ 4.33 eV), again in good

agreement with the average adsorption energy (4.47 eV) from our DFT calculations. Given the close correspondence between the key interaction energies obtained via OPLS-AA and the DFT-calculated average adsorption energies—both with and without an electric field—we are confident that the MD simulation results based on this force field are accurate and reliable.

Furthermore, following the reviewers' suggestions, we conducted experiments to directly verify the distribution of the initial anions. First, we employed quantitative nuclear magnetic resonance (NMR) spectroscopy to monitor the variation in the concentrations of two lithium salts on the anode side during charging. Specifically, we assembled a Li–Li symmetric cell and applied a constant current of 0.2 mA. **FigureS19a-b** illustrate the schematic diagram of the experimental setup, which simulates the charging process of a full cell. After approximately 10 min and 30 min of current application, 0.3 mL of electrolyte was collected from the vicinity of the lithium deposition electrode and mixed with 0.3 mL of deuterated chloroform ($CDCl_3$). The resulting solutions were analyzed by ^{11}B NMR spectroscopy, and the relative contents of the two anions were determined by integrating the corresponding peaks.As shown in **Figures S19c-d**, with increasing lithiation time, the concentration of $ODFB^-$ anions near the lithium-deposition side (anode side) gradually increased, whereas the concentration of BF_4^- anions decreased. This trend is consistent with the predictions from our molecular dynamics (MD) simulations.

We then further examined the nanostructure of the solid electrolyte interphase (SEI) at the electrode/electrolyte interface using cryogenic transmission electron microscopy (Cryo-TEM) (**Figure S29**). The SEI was found to feature an outer layer rich in LiF and an inner layer containing Li_3N and B–O species, which provides additional evidence supporting our design concept.

As the reviewers' comment, the sputtering XPS depth profiling primarily reflect the cumulative decomposition and transport processes of the electrolyte after prolonged cycling, and therefore cannot directly verify the initial anion distribution predicted by the simulations. To address this, we supplemented our study with depth-profiling XPS analyses after different numbers of cycles (1, 20, and 100) (**Figure R1**). The results

showed that, regardless of the number of cycles, the anode interface consistently maintained a nanostructure with an LiF-rich outer layer and an Li_3N/B–O-containing inner layer. This clearly demonstrates that the SEI structure formed in our experimental samples retains excellent integrity throughout cycling.

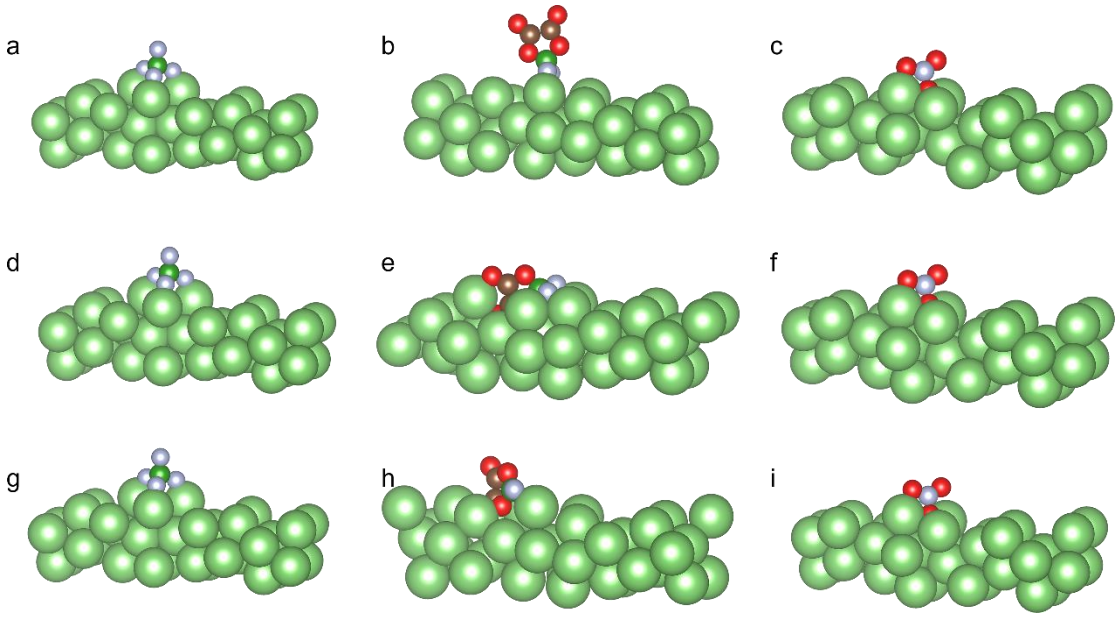

Figure S14. The adsorption energy calculations of three lithium salts — $LiBF_4$ (a, d, g), LiODFB (b, e, h), and $LiNO_3$ (c, f, i) — under three applied electric field conditions: 0 V/nm (a, b, c), −0.1 V/nm (d, e, f), and 1 V/nm (g, h, i).

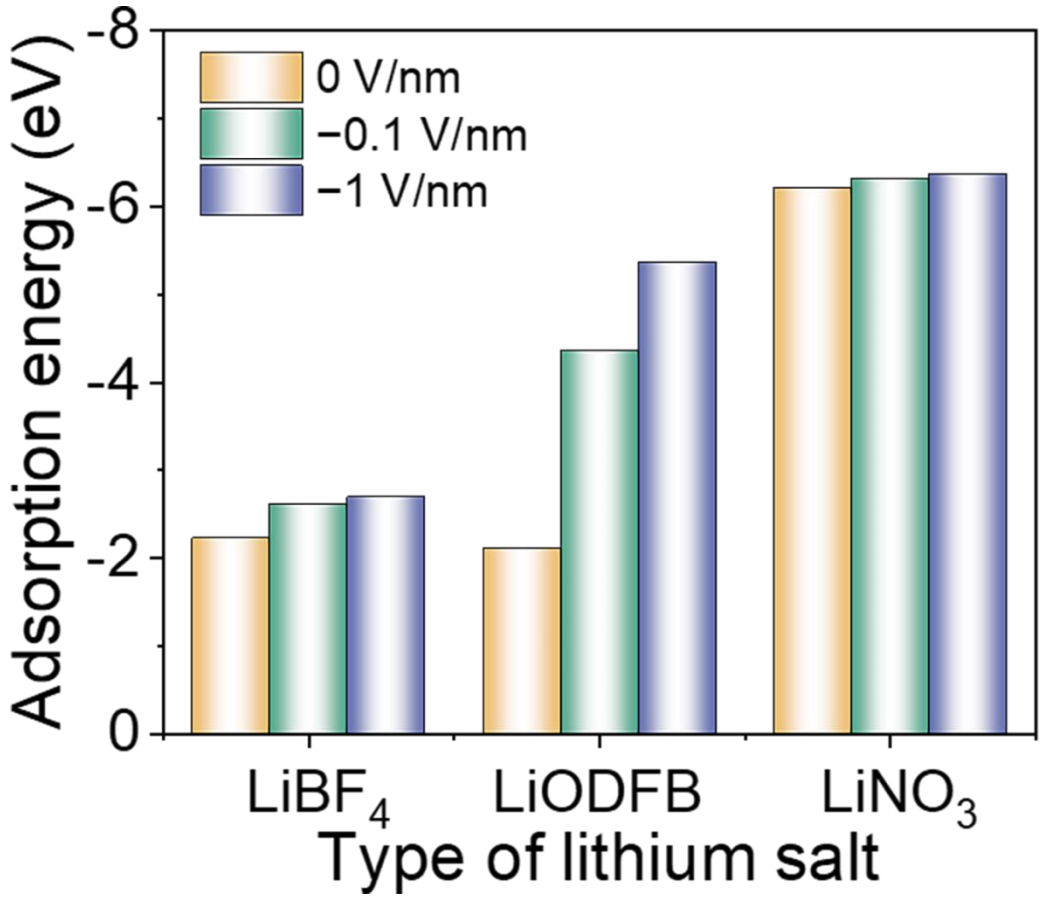

Figure S15. Adsorption energies of different lithium salts under various voltage conditions

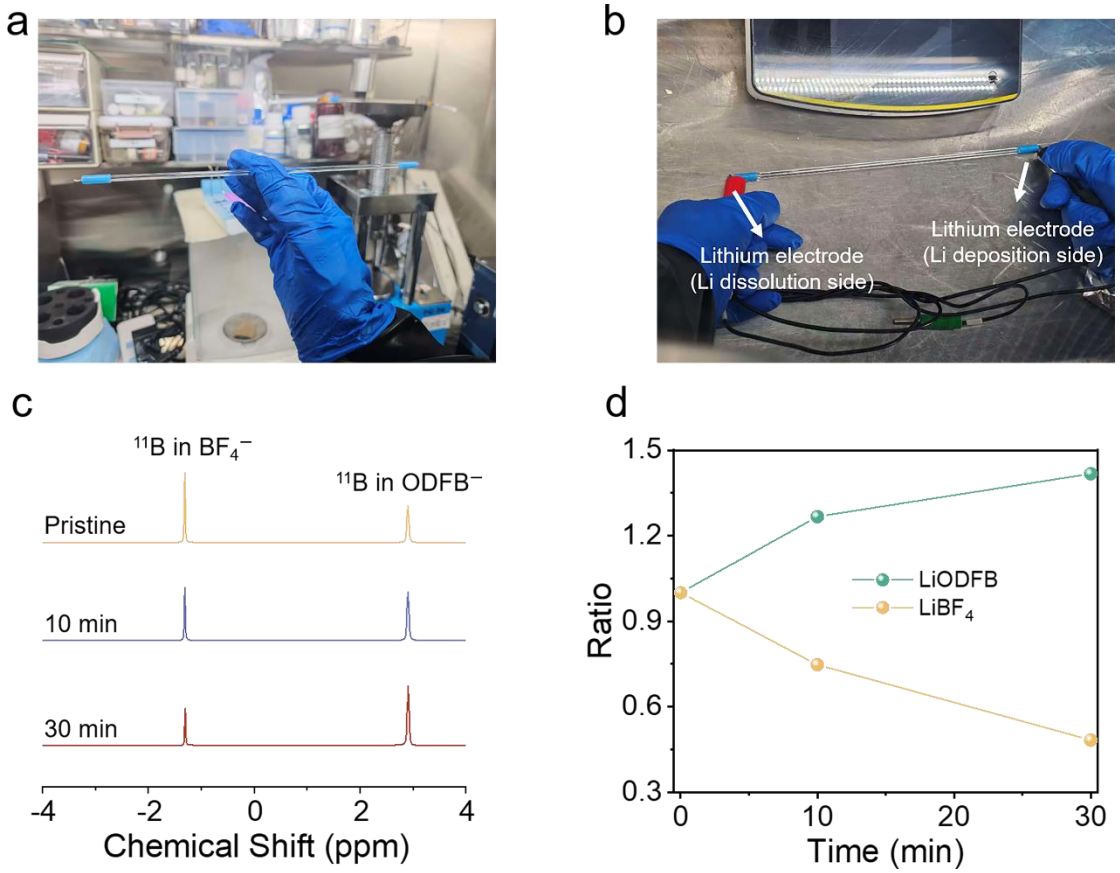

Figure S19. (a, b) Experimental setup for ion migration studies using 0.5 M-DBN electrolyte. (c) Quantitative NMR results showing the electrolyte composition near the lithium deposition electrode. (d) Relative compositional changes in the electrolyte near the lithium deposition electrode.

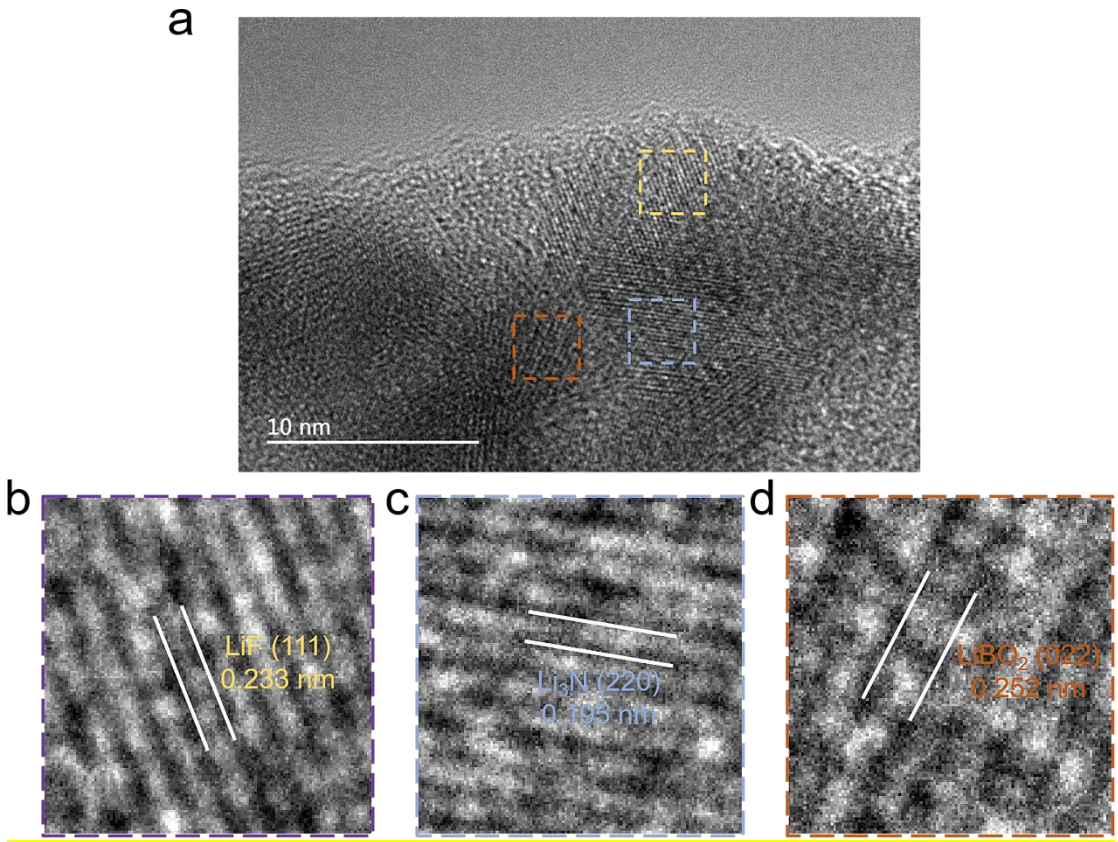

Figure S29. (a) Cryo-TEM image of the SEI formed on lithium metal using the 0.5 M-DBN electrolyte; the colored rectangles indicate the presence of LiF (yellow), Li_3N (blue), and $LiBO_2$ (maroon). The marked regions in the cryo-TEM image (a) are enlarged in (b–d), showing the corresponding nanocrystals of LiF (b), Li_3N (c), and $LiBO_2$ (d), each exhibiting distinct lattice fringes.

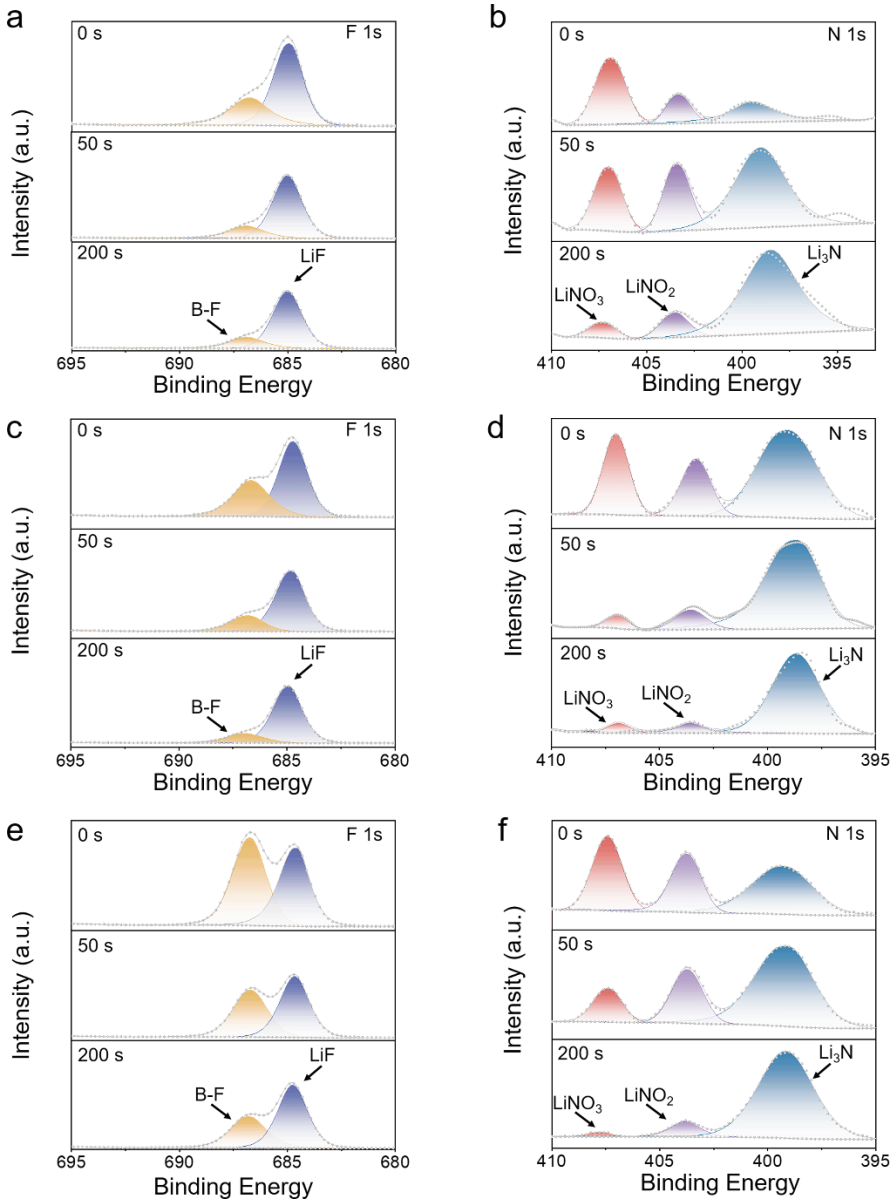

Figure R1. F 1s (a, c, e) and N 1s (b, d, f) XPS spectra of the lithium metal anode interface in Li||NCM811 cells using the 0.5 M-DBN electrolyte after 1 cycle (a, b), 20 cycles (c, d), and 100 cycles (e, f).

2. The proposed link between the initial anion distribution and the long-term SEI layering remains speculative. Continued LiODFB consumption does not ensure sustained interfacial enrichment. Over extended cycling, differences in anion transport properties are likely to dominate, and without direct evidence, the proposed mechanism is not convincingly supported.

Response: We sincerely thank the reviewer for the detailed review of our manuscript. As the reviewer rightly pointed out, the growth of the solid electrolyte interphase (SEI) is indeed a continuous process. However, the consumption of the lithium salt (in this case, lithium difluoro(oxalato)borate, LiODFB) does not occur extensively or uniformly throughout cycling. The critical stage for SEI formation is during the initial few cycles of battery operation, during which LiODFB participates in reactions to form a uniform and stable SEI layer.

Given the electronically insulating nature of SEI, once a complete initial layer is established, electrons can no longer penetrate the interface to trigger further decomposition of the lithium salt. As a result, in subsequent cycles, the evolution of the SEI is primarily driven by the volume changes associated with lithium plating/stripping, which may locally damage the SEI. In such cases, the electrolyte decomposes at these damaged sites to form new SEI layers for "self-repair."

The SEI formed in our study demonstrates excellent elasticity, allowing it to effectively accommodate volume fluctuations during cycling and thereby significantly reduce lithium salt consumption from repeated SEI rupture and repair (**Figure R2**). Furthermore, we conducted XPS characterization of the anode interface after different cycle numbers, and the results show that the SEI composition and structure remain largely consistent throughout cycling. This provides strong evidence supporting our conclusion that once the initial SEI is stably formed, the subsequent lithium salt consumption is substantially reduced (**Figure R1**).

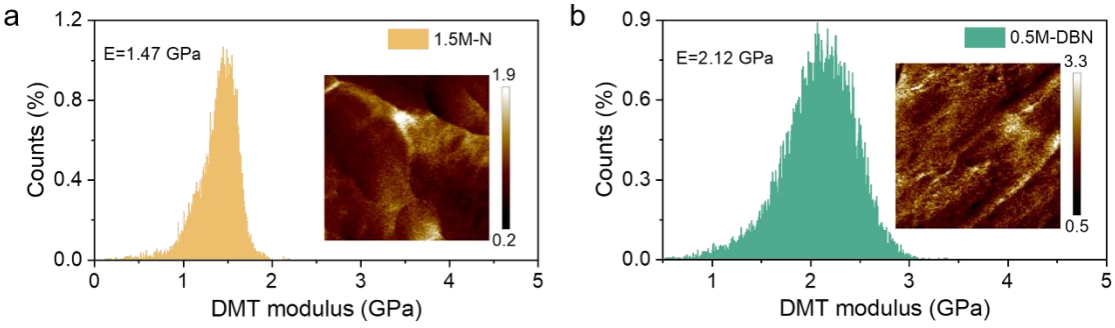

Figure R2. DMT modulus distribution of 1.5 M-N (a) and 0.5 M-DBN (b) SEI.

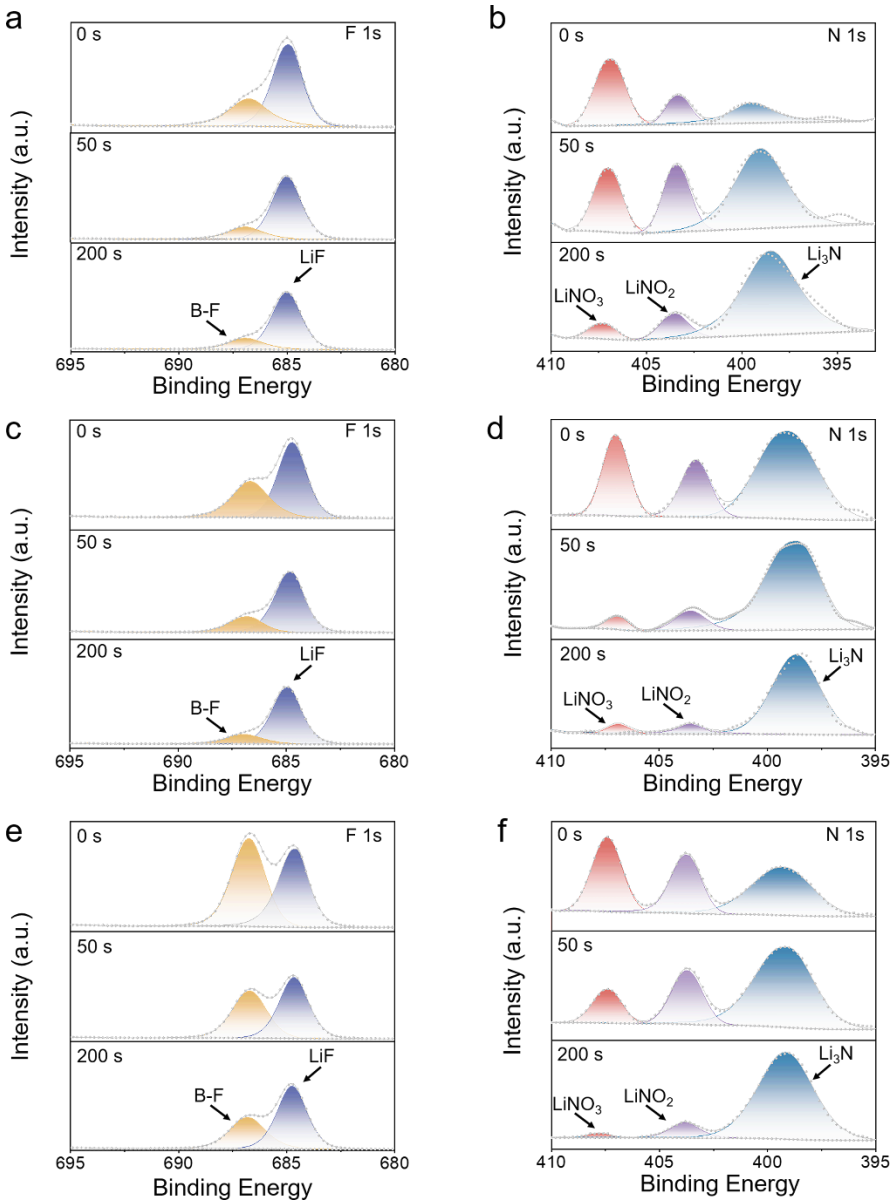

Figure R1. F 1s (a, c, e) and N 1s (b, d, f) XPS spectra of the lithium metal anode interface in Li||NCM811 cells using the 0.5 M-DBN electrolyte after 1 cycle (a, b), 20 cycles (c, d), and 100 cycles (e, f).

3. The two additional binary systems (LiDOB + LiFSI and $LiNO_3$ + LiTFSI) provide some insight but are insufficient to establish the generality of the proposed design principle. Attributing inner-layer formation to LiDOB or $LiNO_3$ decomposition based solely on Li_2O detection is unconvincing, as Li_2O can also result from the decomposition of imide-based salts such as LiFSI or LiTFSI. This overlap in decomposition pathways limits the interpretability of the experimental evidence.

Without further mechanistic clarification, the claim of a general design principle remains premature.

Response: We thank the reviewer for the careful evaluation of our manuscript. We fully agree with the reviewer's opinion that, in our previous study involving the $LiNO_3$ + LiTFSI system, attributing the formation of Li_2O solely to the decomposition of $LiNO_3$ may be inappropriate.

To further validate the universality of the proposed mechanism—namely, that differences in anion binding energy drive their competitive adsorption and preferential decomposition near the lithium metal surface—we specifically designed two entirely new electrolyte systems, distinct from those used in previous studies:

1. 0.5 M LiBOB / 0.5 M $LiPF_6$ in TEP: In this system, the binding energy of LiBOB is higher than that of $LiPF_6$.
2. 0.5 M $LiNO_3$ / 0.5 M $LiPF_6$ in TEP: In this system, the binding energy of $LiNO_3$ is higher than that of $LiPF_6$.

We subsequently conducted XPS characterization of the lithium metal anode interface to investigate the SEI structures formed in each system:

- **For the LiBOB/$LiPF_6$ system:** According to our theory, LiBOB, having a higher binding energy, preferentially enriches near the lithium metal surface and decomposes first, forming a B–O-rich inner SEI. In contrast, $LiPF_6$, with a lower binding energy, tends to form an outer SEI enriched in LiF. This layered SEI structure was confirmed by depth-profiling XPS analysis, which revealed a B–O-rich inner layer and a LiF-rich outer layer (**Figure R3a-b**).
- **For the $LiNO_3$/$LiPF_6$ system:** Similarly, based on our proposed mechanism, $LiNO_3$ (higher binding energy) decomposes preferentially near the lithium surface, resulting in a significantly higher Li_3N content in the inner SEI compared to the outer layer. Meanwhile, $LiPF_6$ contributes mainly to the formation of a LiF-rich outer SEI. The depth-profiling XPS results of this system were also consistent with the predicted spatial distribution (**Figure R3c-d**).

Overall, these experimental results provide strong evidence that the anion gradient distribution mechanism we have uncovered is not a phenomenon specific to a particular electrolyte system, but rather a universally applicable interfacial regulation principle.

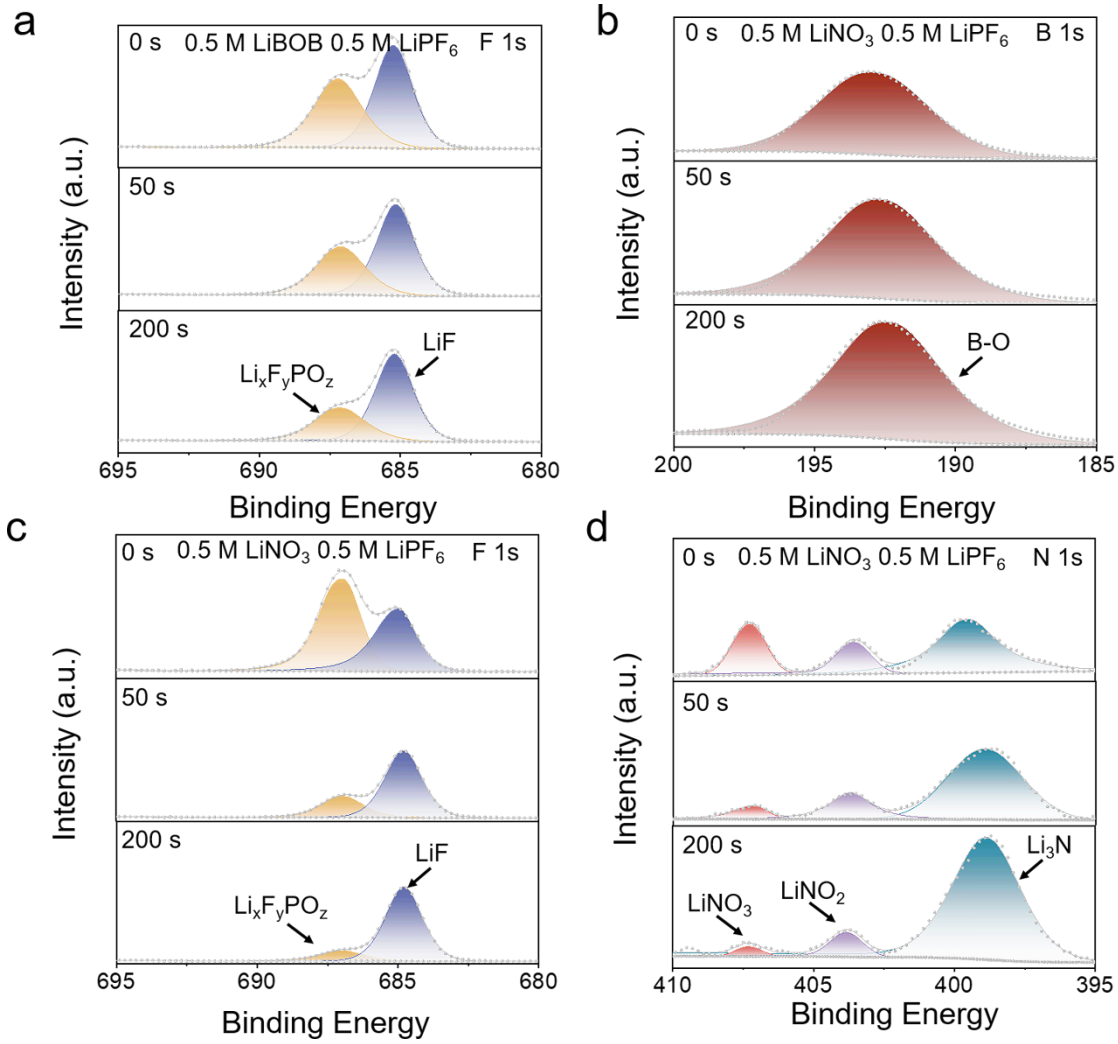

Figure R3. (a) F1s and (b) B1s XPS spectra of the SEI formed in the 0.5 M LiBOB + 0.5 M $LiPF_6$ TEP electrolyte. (c) F1s and (d) N1s XPS spectra of the SEI formed in the 0.5 M $LiNO_3$ + 0.5 M $LiPF_6$ TEP electrolyte.

Reviewer #3 (Remarks to the Author):

The authors provide detailed response to the reviewer's comment. The "voltage-driven anion migration" strategy was further discussed in details in the revised manuscript, which may promote the development of phosphate electrolyte. Some remaining points need to be addressed.

Response: Many thanks for the referee's valuable suggestion, especially, the insightful comments for further improving the quality of the manuscript. We have carefully addressed the issues as follows.

1. The experimental evidence of dual-layer SEI is not convincing. XPS was used in the manuscript to verify the dual-layer feature of SEI, which is a key finding of this work. However, XPS results can be misleading sometime, where the sputtering is not homogeneous among different components, undermining the claim of dual-layer SEI formation. To clearly demonstrate the dual-layer feature of SEI, cryogenic electron characterization is suggested.

Response: We appreciate the reviewer's careful evaluation of our manuscript. As reviewer rightly pointed out, XPS analysis may suffer from reliability issues due to possible artifacts introduced during sputtering. To address this concern, we followed the reviewer's suggestion and employed cryogenic transmission electron microscopy (Cryo-TEM) for further characterization.

As shown in **Figure S29a**, the SEI layer formed using the 0.5 M-DBN electrolyte exhibits a dense, inorganic-rich morphology on the lithium metal surface. High-resolution analysis identified several crystalline components within the SEI, including the LiF (111) plane with a lattice spacing of 0.233 nm, the Li_3N (220) plane (0.195 nm), and the $LiBO_2$ (022) plane (0.252 nm), as displayed in **Figures S29b–d**. These observations reveal a distinct layered structure: the inner SEI region is primarily composed of Li_3N and $LiBO_2$, while the outer layer is dominated by LiF. This spatial distribution is fully consistent with our earlier XPS depth profiling and TOF-SIMS results. Noted. In lines 204–205, the manuscript states: "*Furthermore, the presence of this bilayer SEI structure was corroborated by cryo-electron microscopy observations (Figures S29).*"

Such a stratified SEI structure offers synergistic advantages: the outer LiF layer provides high interfacial rigidity that effectively suppresses lithium dendrite growth,

whereas inner compounds like Li_3N exhibit high Li^+ conductivity, enhancing ionic transport through the SEI. Additionally, the presence of B–O bonded components contributes to mechanical flexibility. Together, these features enable the formation of a robust SEI with both high ionic conductivity and mechanical adaptability, facilitating dense lithium deposition and significantly improving plating/stripping efficiency.

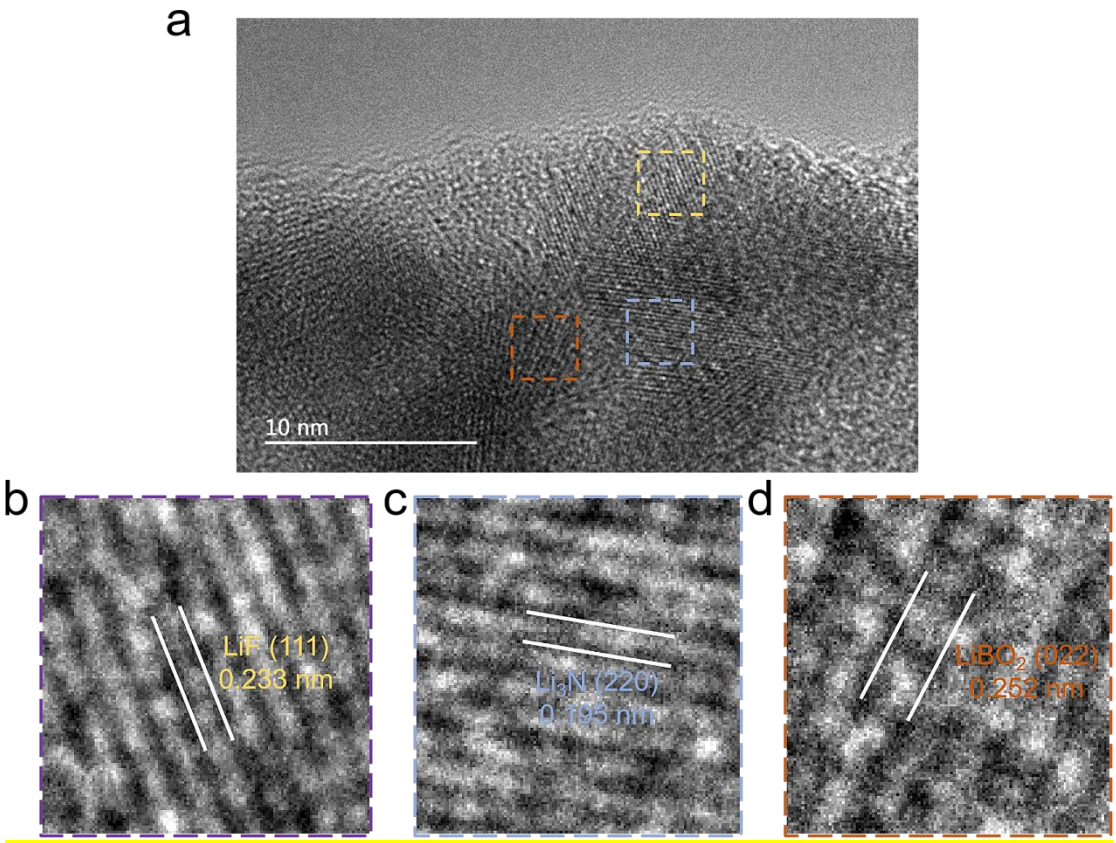

Figure S29. (a) Cryo-TEM image of the SEI formed on lithium metal using the 0.5 M-DBN electrolyte; the colored rectangles indicate the presence of LiF (yellow), Li_3N (blue), and $LiBO_2$ (maroon). The marked regions in the cryo-TEM image (a) are enlarged in (b–d), showing the corresponding nanocrystals of LiF (b), Li_3N (c), and $LiBO_2$ (d), each exhibiting distinct lattice fringes.

2. The applicability of the so-called “voltage-driven anion migration” strategy in Li metal full cell should be fully charified. This manuscript reports a voltage-based strategy to regulate SEI. However, it is known that Li chemically reacts with electrolyte to form an SEI before cycling, i.e., before applying the electric field. Such a chemically formed SEI may substantially affect the “voltage-driven anion migration” strategy to

regulate the SEI structure. The compasion between reported electrolyte and traditional carbonate electrolyte is not very convincing.

Response: We sincerely thank the reviewer for the thoughtful and detailed comments. As correctly noted, prior to battery cycling, lithium metal spontaneously reacts with the electrolyte to form a chemically driven solid electrolyte interphase (SEI) that is extremely thin, structurally loose, and disordered (ACS Energy Letters, 2024, 9(11), 5268–5278). Although this chemically formed SEI can offer an initial barrier against further electrolyte decomposition, its high porosity and limited blocking ability result in poor stability, rendering it vulnerable to subsequent electrochemical reconstruction. With the application of external potential during charge/discharge processes, further electrochemical reduction of the electrolyte occurs, leading to the formation of a second SEI layer on top of the initial chemical SEI. This electrochemically dominated SEI is typically denser and more functionalized. The electrochemical formation stage largely determines the final thickness, compactness, and composition of the SEI, which in turn critically influences long-term cycling performance (Batteries & Supercaps, 2021, 4, 909; Small, 2020, 16(23), e2000756; Energy Environ. Sci., DOI: 10.1039/D5EE01030F).

As the reviewers' suggestion, we prepared a control electrolyte system consisting of 0.75 M LiODFB/EC-DMC and 0.75 M $LiBF_4$/EC-DMC (it should be noted that $LiNO_3$ was excluded from this control system due to its insolubility in the EC/DMC solvent). The comparative experiments were conducted under two different conditions: 4.3 V at 1C and 4.5 V at 0.5C. As shown in **Figure R4**, under the 4.3 V, 1C condition, the 0.5 M-DBN electrolyte exhibited excellent cycling stability, retaining 87.90% of its initial capacity after 900 cycles. In contrast, the capacity retention of the 0.75 M LiODFB + 0.75 M $LiBF_4$/EC-DMC electrolyte was only 36.97%. Under the higher voltage condition of 4.5 V, the 0.5 M-DBN electrolyte maintained 90.91% capacity retention after 600 cycles.

Furthermore, to investigate the influence of different electrolyte systems, comparative experiments were performed using lithium sulfonylimide-based

electrolytes, including 1.5 M LiFSI/TEP, 1.5 M LiTFSI/TEP, 1.5 M LiFSI/EC-DMC, and 1.5 M LiTFSI/EC-DMC.

The results showed that all four systems exhibited insufficient cycling performance. Specifically, 1.5 M LiFSI/EC-DMC displayed a voltage plateau stagnation during the initial charging stage, likely due to severe oxidative decomposition (**Figure R5a**). Although 1.5 M LiTFSI/EC-DMC completed charge–discharge cycles, its capacity rapidly decayed within 100 cycles (**Figure R5b**). Both 1.5 M LiFSI/TEP and 1.5 M LiTFSI/TEP showed low initial capacities and rapid capacity fading (**Figures R5c-d**).

These comparative results clearly demonstrate the significant advantages of the 0.5 M-DBN electrolyte in cycling stability and high-voltage tolerance, strongly validating our electrolyte design strategy.

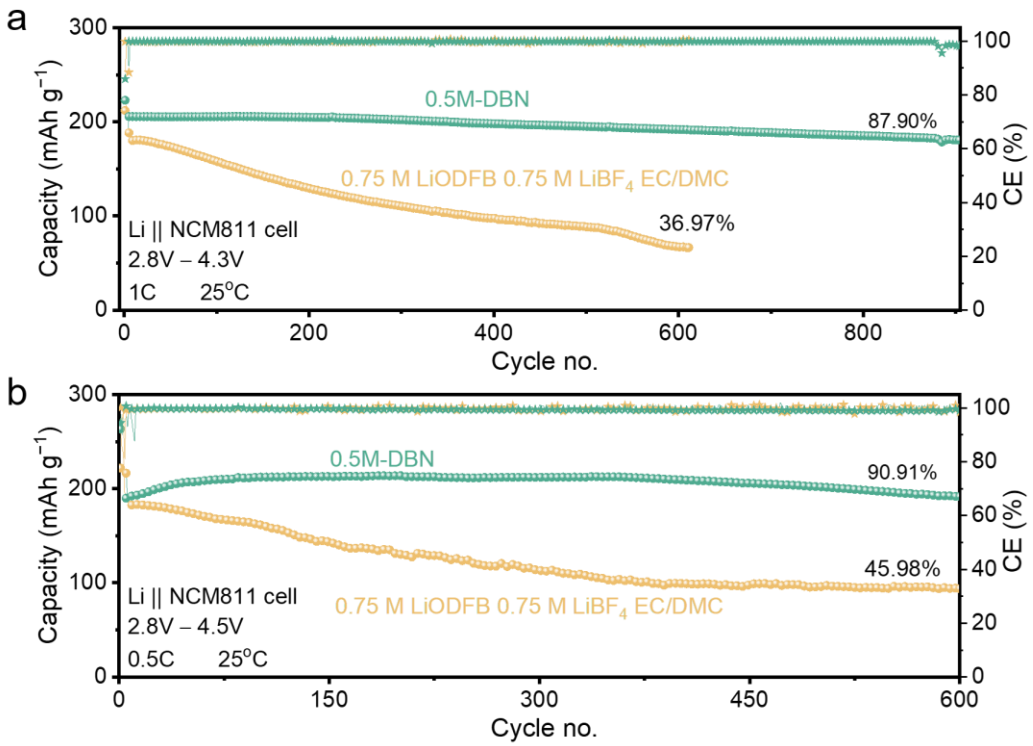

Figure R4. Comparison of the cycling performance of the two electrolytes under (a) 4.3 V at 1C and (b) 4.5 V at 0.5C conditions.

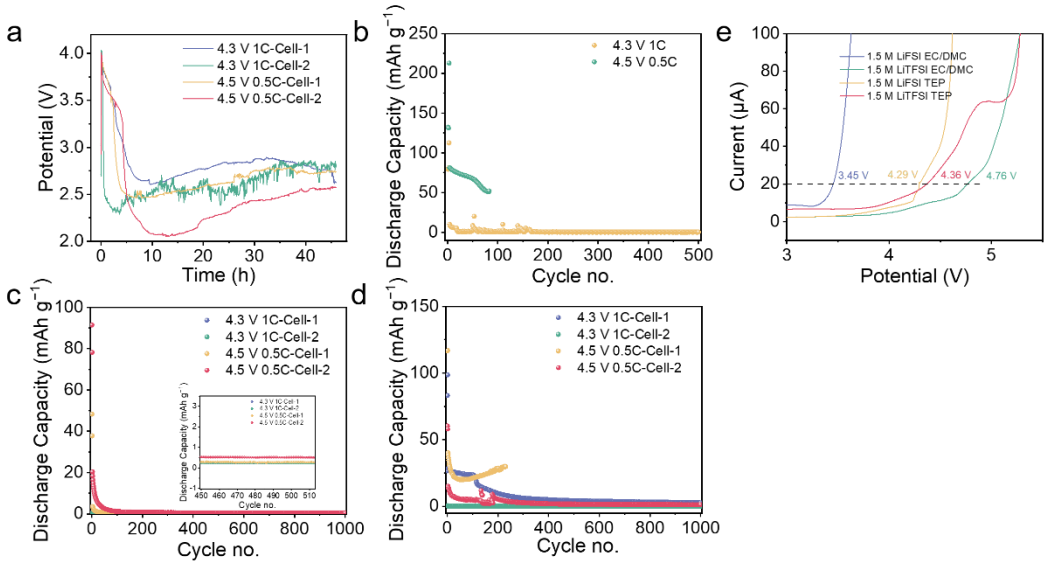

Figure R5. (a) Time–voltage profile of the first cycle for the 1.5 M LiFSI/EC-DMC electrolyte. (b) Cycling performance of the 1.5 M LiTFSI/EC-DMC electrolyte under 4.3 V 1C and 4.5 V 0.5C conditions. (c) Cycling performance of the 1.5 M LiFSI/TEP electrolyte under 4.3 V 1C and 4.5 V 0.5C conditions. (d) Cycling performance of the 1.5 M LiTFSI/TEP electrolyte under 4.3 V 1C and 4.5 V 0.5C conditions. (e) Linear sweep voltammetry (LSV) curves of the four electrolytes.

3. The FTIR results need more detailed discussion. Please provide references for each peak's attribution in the profiles. In particular, the peak position of LiF needs to be checked. Meanwhile, the curve change during charge and discharge process is not very clear, since most of curves overlap in Fig. 2a.

Response: We sincerely thank the reviewer for the careful evaluation of our manuscript. In light of your professional guidance, we have we have conducted a more detailed discussion of the FTIR results in the revised manuscript "*As shown in Figures 2a and S20, during the lithium deposition stage (i.e., the desolvation process), the pronounced depletion peaks at 977.90 cm^{-1} (P–O–C) and 1255.31 cm^{-1} (P=O) correspond to the gradual consumption of solvated TEP, while the emerging peak at 958.62 cm^{-1} (P–O–*

C) indicates the release of desolvated solvent molecules at the electrode interface[14]. Figure S19 presents the in-situ infrared spectra of the 1 M $LiPF_6$/EC–DMC electrolyte system along with the corresponding spectral analysis." in **Lines 148-154**. Furthermore, the assignments of each peak in the in situ FTIR spectra and the corresponding references are as follows: the characteristic peak of LiF appears at 837 cm^{-1} (Reference: Nat. Commun. 13, 1398 (2022)); the peaks corresponding to P–O–C, B–O–R, and P=O are located at approximately 980 cm^{-1}, 1020 cm^{-1}, and 1260 cm^{-1}, respectively (Reference: Energy Storage Materials 42, 628–635 (2021)).

Regarding the reviewer's concern about the insufficiently clear spectral changes in the in situ FTIR curves, we fully understand this issue. We previously attempted to present the data as contour maps to better illustrate the trends; however, the outcome was unsatisfactory. This was mainly due to baseline inconsistencies in the current in situ FTIR dataset (as indicated by the dashed box region in **Figure R6a**, where substantial baseline variations exist during the initial charge/discharge stages). If we forcibly normalize the baseline to generate contour plots, subtle signals—such as the LiF peak at ~833 cm^{-1}—would be obscured. Additionally, the baseline mismatch leads to difficulty in visualizing downward-oriented (i.e., product) peak evolutions in the contour format (**Figure R6b**). It is worth noting that the data presented in **Figure 7b** have already undergone a minimal baseline correction. More aggressive baseline normalization could distort peak intensities and compromise data reliability. Nevertheless, we have also provided individual spectra for the lithiation and delithiation stages below the full charge/discharge curves (**Figure R7**). These plots allow for more distinct observation of the evolution of key characteristic peaks.

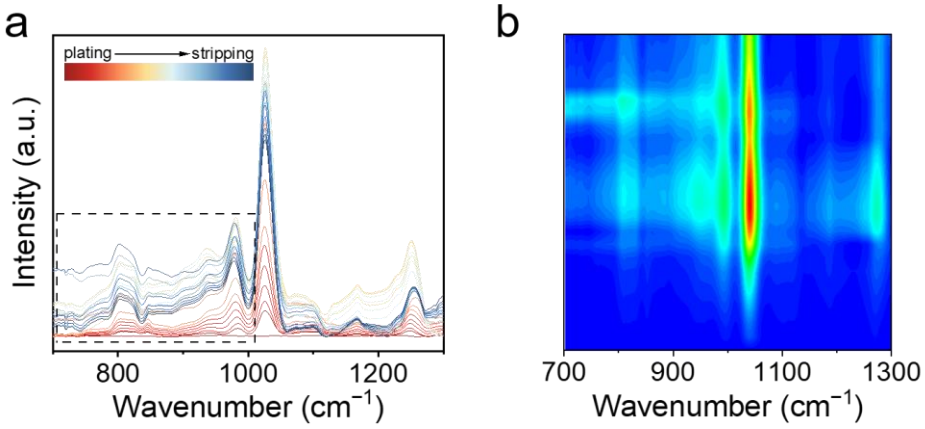

Figure R6. (a) Stacked in situ infrared spectra of the 0.5 M-DBN electrolyte. (b) Contour plot of the in situ infrared spectra for the 0.5 M-DBN electrolyte.

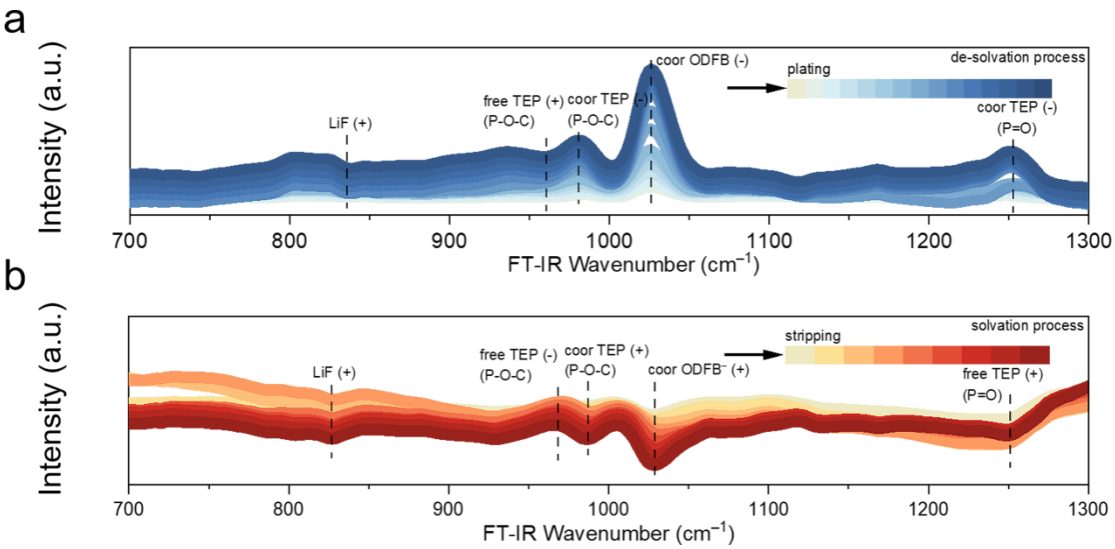

Figure R7. Stacked plots of the in-situ infrared spectra during the plating (a) and stripping (b) stages.

4. The formation mechanism of dual-layer SEI remains not very clear. It was found that DFOB- can be decomposed to form B-O species in the inner SEI. In principle, DFOB- can decompose to form LiF in the meantime, but the inner SEI lacks LiF. Why can't we detect large amount of LiF in the inner layer?

Response: Thank you to the reviewer for the careful evaluation of our manuscript. We fully understand the concern that LiODFB decomposition might theoretically generate LiF. However, based on bond dissociation energy analysis, the B–O bond in the difluoro(oxalato)borate anion ($DFOB^-$) of LiODFB has a much lower bond energy (210.7 kJ mol^{-1}), and in its radical form (DFOB•), the B–O bond energy can be as low as –50.1 kJ mol^{-1} (references: Nat. Energy 3, 739–746 (2018); ACS Appl. Mater. Interfaces 2018, 10 (3), 2469–2479). This suggests that the B–O bond is highly susceptible to cleavage, especially in the radical state, leading to the formation of B–O-rich decomposition products in the SEI.

In contrast, the B–F bond possesses significantly higher bond dissociation energy—575.3 kJ mol^{-1} in the anion and 236.4 kJ mol^{-1} in the radical—which is far greater than that of the B–O bond. Therefore, the decomposition of LiODFB preferentially involves B–O bond cleavage and does not produce LiF in large quantities.

To validate this mechanism, we formulated a 1.5 M LiODFB in TEP electrolyte and performed sputtering XPS depth profiling of the Li metal interface. The results revealed that B–O species are enriched in the inner SEI layer, while LiF is predominantly located in the outer SEI region. This spatial distribution pattern is fully consistent with the decomposition pathway we proposed based on bond energy differences (**Figure R8**).

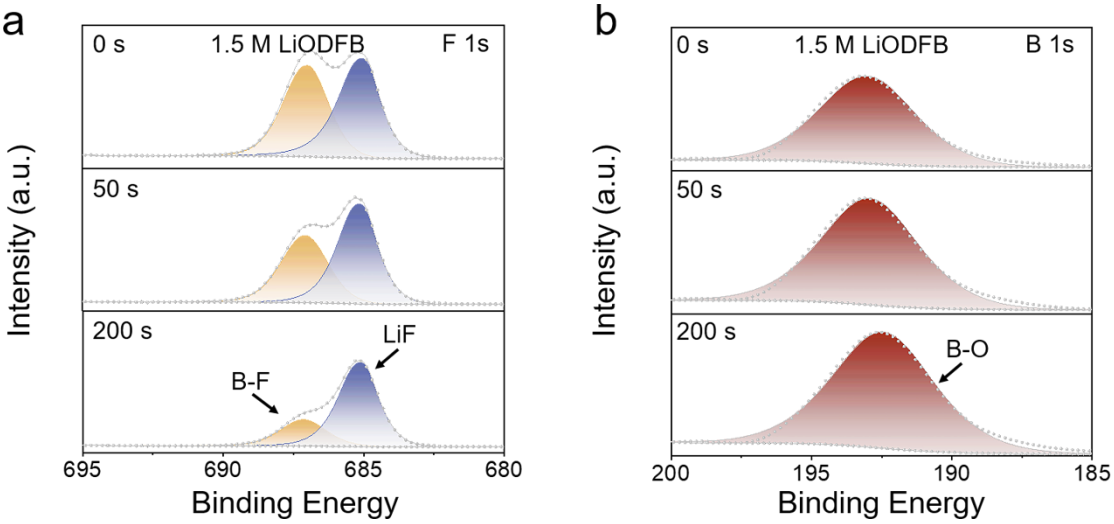

Figure R8. (a) F1s and (b) B1s XPS spectra of the SEI formed in the 1.5M LiODFB TEP electrolyte.

5. In Fig. 1f, it can be seen that the solvent TEP dominates on the Li surface. Since all of electrolyte components, including TEP, BF4-, DFOB- and NO3-, can decompose on Li surface, more TEP corresponds to more severe TEP decomposition. How can those minor species (anions) on Li surface can protect Li metal from reactive phosphate?

Response: We thank the reviewer for their careful evaluation of our manuscript. As shown in **Table S1**, TEP is indeed the dominant component in the electrolyte, and as the reviewer rightly pointed out, it constitutes the major species at the interface. However, since the LUMO energy levels of the anions are lower than that of TEP, the anions preferentially undergo decomposition at the interface, leading to the formation of an inorganic-rich interfacial layer. This layer effectively prevents direct contact between TEP and the lithium metal, thereby reducing the reactivity of TEP.

Table S1. Detailed components of the four MD models

Components	TEP	LiODFB	$LiBF_4$	$LiNO_3$
0.5 M LiODFB+0.5 M $LiBF_4$ +0.5 M $LiNO_3$ in TEP (mmol)	5.9	0.5	0.5	0.5
Molecule number	589.0	50.0	50.0	50.0

Reviewer #1 (Remarks to the Author):

I thank the authors for their comprehensive revisions and additional analyses, which have considerably strengthened the manuscript. In addition, I would ask the authors to address the following points.

Response: Many thanks for the referee's valuable suggestion, especially, the insightful comments for further improving the quality of the manuscript. We have carefully addressed the issues as follows.

1. The finding that OPLS-AA can describe the interaction between Li metal and Li ions with accuracy comparable to DFT is indeed surprising. Could the authors clarify whether the Lennard–Jones parameters for Li metal were specifically adjusted in this work, or whether they were taken directly from previous literature? For the sake of reproducibility and transparency, it is essential that the full set of Lennard–Jones parameters used in the simulations be included in the Supplementary Information. Furthermore, the computational details of the DFT calculations performed for validation are not currently provided in the Supplementary Information. These details must be explicitly included to allow the results to be properly assessed and reproduced.

Response: We thank the reviewer for pointing out the need for clarification regarding the force field parameters and DFT calculation details. To ensure reproducibility and transparency, we have included in the revised Supplementary Information (SI) a complete list and explanation of all Lennard–Jones (LJ) parameters and charge assignments used in this work, along with the full computational settings and key input files employed in the validating DFT calculations. Noted SI. In lines 122–136, the manuscript states: *"The density functional theory (DFT) calculation implemented in the Vienna Ab initio simulation package (VASP) was conducted to study adsorption energy. The exchange-correlation potential was described by using the generalized gradient approximation of Perdew-Burke-Ernzerhof (GGA-PBE). The projector augmented-wave (PAW) method was employed to treat interactions between ion cores and valence electrons. We simulated the voltage effect by applying an external electric field of 0,*

−0.1 and −1 V/nm along the vacuum direction. The plane-wave cutoff energy was fixed to 450 eV. Given structural models were relaxed until the Hellmann–Feynman forces smaller than −0.02 eV Å^{-1} and the change in energy smaller than 10^{-5} eV was attained. Grimme's DFT-D3 methodology was used to describe the dispersion interactions among all the atoms in adsorption models. For searching the transition states, we employed the nudged elastic band (NEB) method as implemented in VASP. The adsorption energy of these systems was calculated via following formula:

$$E(binding) = E(A) + E(B) - E(AB).$$

In which, E(binding) is the adsorption energy, E(A), E(B), E(AB) are the single-point energy of the various substrates."

Table S6. Lennard-Jones parameters[S18-S19]

atom	σ (nm)	ε (KJ/mol)	Charge (e)
Li^+			
Li^+	0.21645	0.0764793	0.80
BF_4^-			
B	0.35814	0.39748	0.6620
F	0.31181	0.25104	−0.3655
F	0.31181	0.25104	−0.3655
F	0.31181	0.25104	−0.3655
F	0.31181	0.25104	−0.3655
NO_3^-			
N	0.315	0.71128	0.6352
O	0.286	0.87864	−0.4784
O	0.286	0.87864	−0.4784
O	0.286	0.87864	−0.4784
$DFOB^-$			
C	0.39967	0.359824	0.6604
C	0.39967	0.359824	0.6604
O	0.296	0.87864	−0.5376
O	0.296	0.87864	−0.5376
OS	0.300	0.71128	−0.5950
OS	0.300	0.71128	−0.5950
B	0.364	0.75312	1.0392

F	0.312	0.255224	−0.4474
F	0.312	0.255224	−0.4474
TEP			
P	0.374	0.8368	2.1376
O	0.296	0.87864	−0.9188
O1	0.290	0.58576	−0.6499
O1	0.290	0.58576	−0.6803
O1	0.290	0.58576	−0.7062
C	0.350	0.276144	−0.0101
C	0.350	0.276144	−0.2477
C	0.350	0.276144	−0.0357
C	0.350	0.276144	−0.2471
C	0.350	0.276144	−0.0016
C	0.350	0.276144	−0.3275
H	0.250	0.12552	0.1151
H	0.250	0.12552	0.1151
H	0.250	0.12552	0.1046
H	0.250	0.12552	0.1046
H	0.250	0.12552	0.1046
H	0.250	0.12552	0.1043
H	0.250	0.12552	0.1043
H	0.250	0.12552	0.1069
H	0.250	0.12552	0.1069
H	0.250	0.12552	0.1069
H	0.250	0.12552	0.1349
H	0.250	0.12552	0.1349
H	0.250	0.12552	0.1147
H	0.250	0.12552	0.1147
H	0.250	0.12552	0.1147
Li_subs			
Li	0.280	9.00	0

2. I remain unconvinced by the manuscript's conclusion that differences in anion adsorption strength within 1 nm of the Li metal surface directly determine the SEI structure extending over tens of nanometers. Even if the adsorbed anions decompose during the initial stages of SEI formation, subsequent processes such as ion transport are also involved in SEI growth. Therefore, it does not seem reasonable to directly link the initial local adsorption state to the final SEI architecture. A clear rationale is required

to bridge this scale gap and substantiate the proposed mechanism.

Response: We sincerely thank the reviewer for the careful evaluation of our manuscript and for the insightful and constructive comments. As you have correctly pointed out, there exists a complex physicochemical process bridging the initial atomic-scale adsorption events and the subsequent mesoscopic formation of the SEI, and that directly correlating the two indeed requires a more rigorous justification. In our work, we emphasized that the initial anion adsorption and decomposition behavior establishes the critical starting conditions for heterogeneous SEI nucleation and growth. We agree with your viewpoint that a complete mechanism must incorporate the subsequent processes. Nevertheless, different anion adsorption strengths result in initial SEIs with distinctly different chemical compositions and properties. Specifically, due to the stronger adsorption affinity and lower LUMO levels of LiODFB and $LiNO_3$, their decomposition preferentially forms an inorganic-rich and compact inner layer, whereas the weaker adsorption of $LiBF_4$ instead favors the formation of an outer LiF layer. In the subsequent cycling process, the distribution state of anions is preserved, such that the newly formed SEI in the fractured regions retains the original compositional characteristics: a B–O- and Li_3N-rich inner layer, and a LiF-dominated outer layer. This mechanism effectively ensures the overall uniformity and structural stability of the SEI.

At the same time, we acknowledge that our theoretical simulations were conducted in relatively small simulation cells. If extended to the scale of a full practical cell, such concentration gradients would likely become more pronounced, thereby further enhancing the stratified SEI structure. Furthermore, our experimental characterizations—including sputtering XPS (**Figure 2c-e**), TOF-SIMS (**Figure 2h-i**), and Cryo-TEM (**Figure S29**)—have confirmed the successful construction of the envisioned triple-layer SEI and demonstrated that it remains stable throughout extended cycling (**Figure R1**).

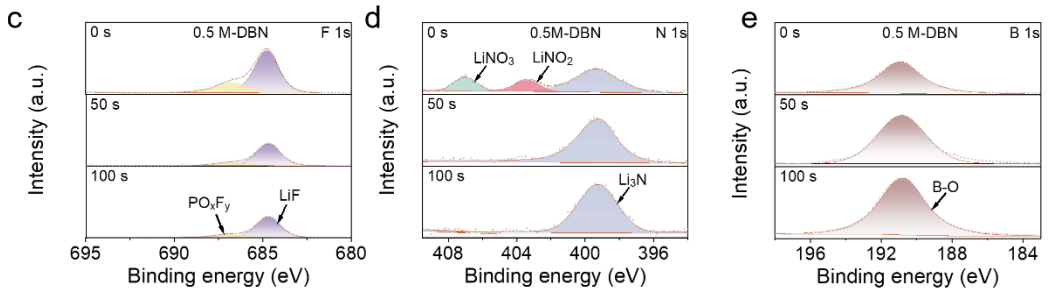

Figure 2c-e. XPS depth profiles were determined of (c) F1s, (d) N1s, and (e) B1s of lithium metal anodes recovered from full cell cycled with 0.5 M-DBN electrolyte at sputtering times of 0, 50, and 100 s, respectively.

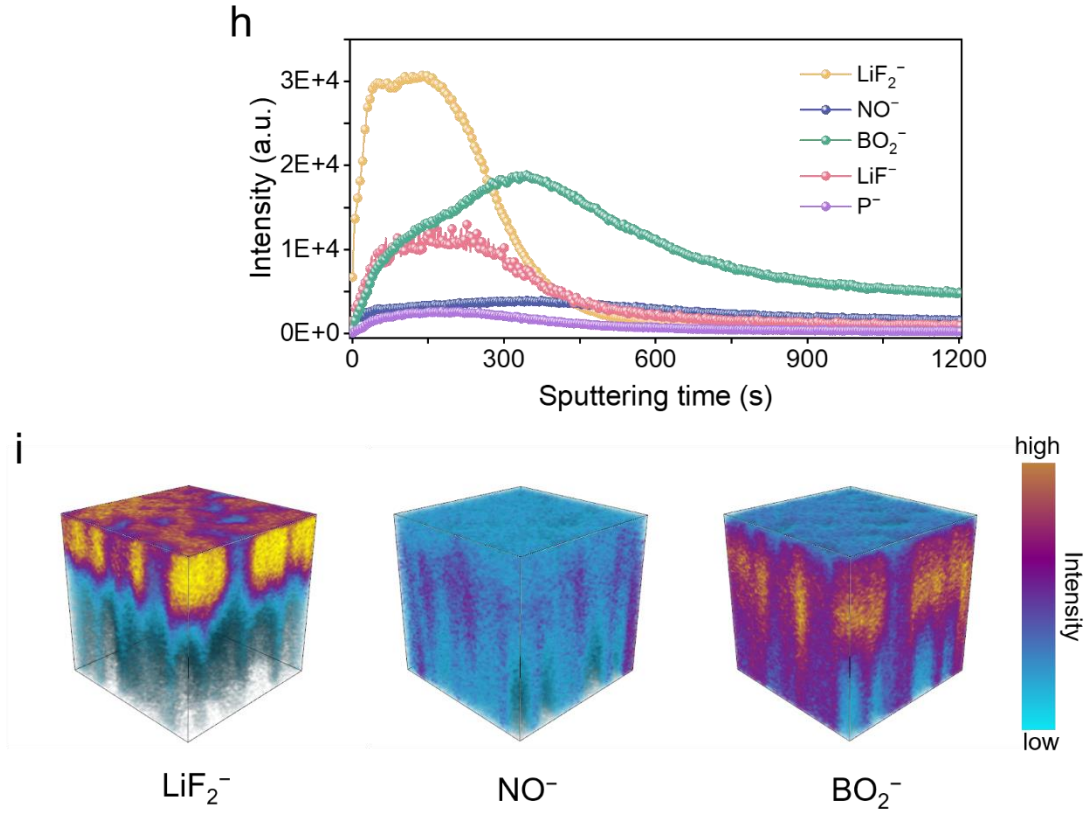

Figure 2h-i. Time-of-flight Secondary Ion Mass Spectrometry (TOF-SIMS) depth distributions (h) and three-dimensional images of various species (i) within a 0.5 M-DBN electrolyte.

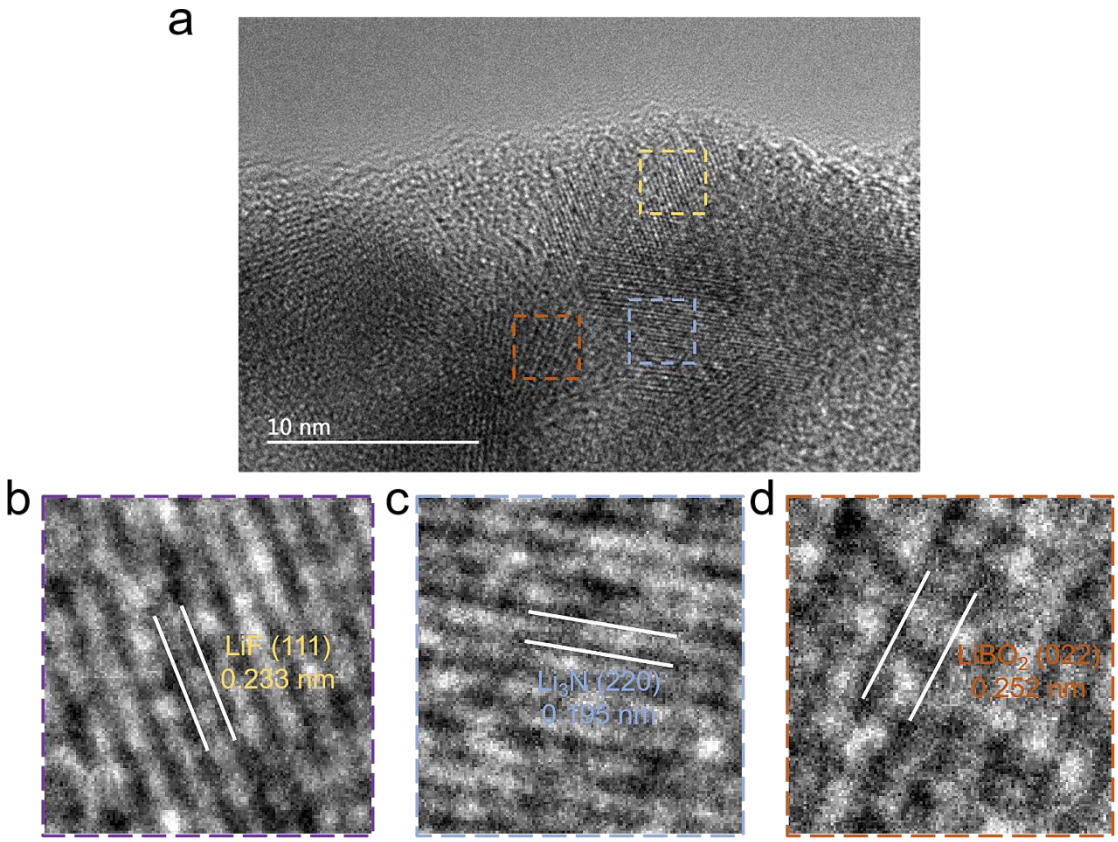

Figure S29. (a) Cryo-TEM image of the SEI formed on lithium metal using the 0.5 M-DBN electrolyte; the colored rectangles indicate the presence of LiF (yellow), Li_3N (blue), and $LiBO_2$ (maroon). The marked regions in the cryo-TEM image (a) are enlarged in (b–d), showing the corresponding nanocrystals of LiF (b), Li_3N (c), and $LiBO_2$ (d), each exhibiting distinct lattice fringes.

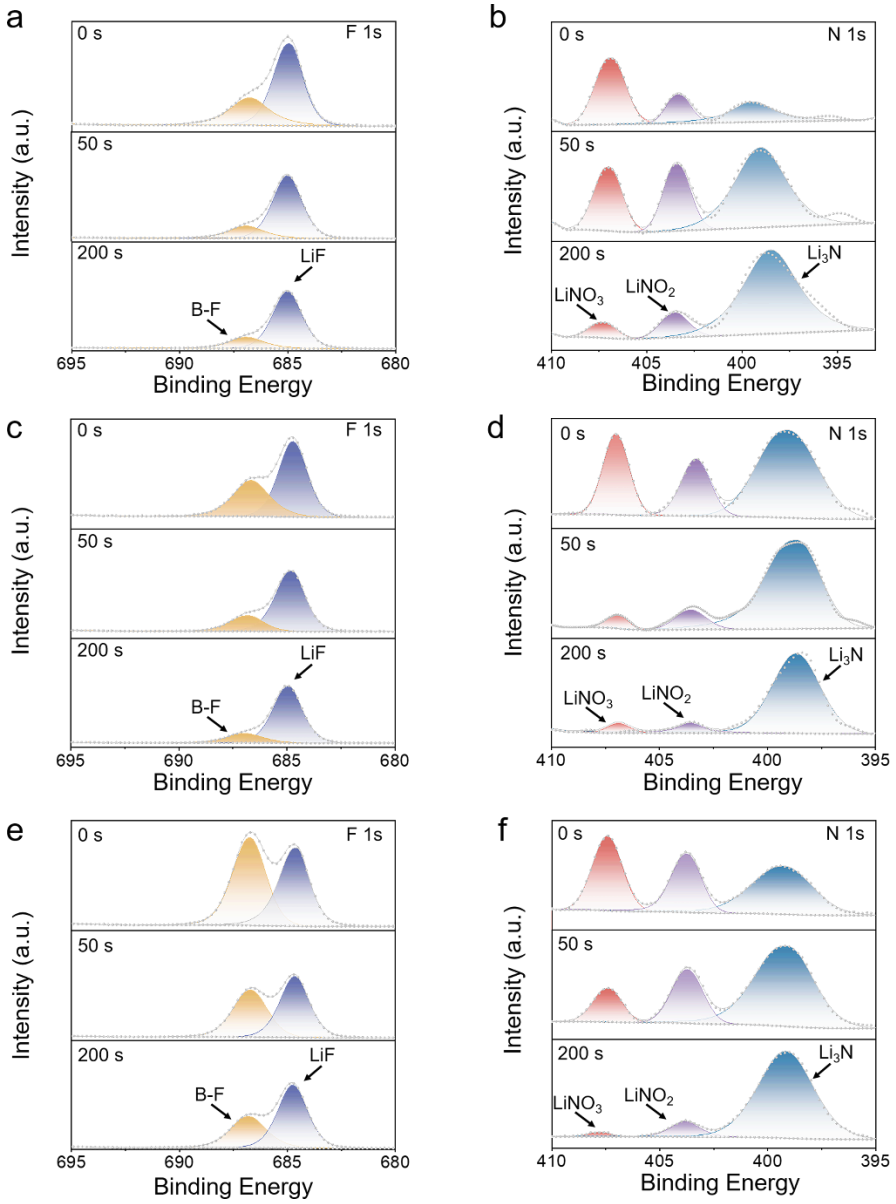

Figure R1. F 1s (a, c, e) and N 1s (b, d, f) XPS spectra of the lithium metal anode interface in Li||NCM811 cells using the 0.5 M-DBN electrolyte after 1 cycle (a, b), 20 cycles (c, d), and 100 cycles (e, f).

Minor comment: Please change the frame color in Fig. S29b to yellow.

Response: We are grateful to the reviewer for the insightful comments. In accordance with the suggestion, the frame color in Figure S29b has been corrected.

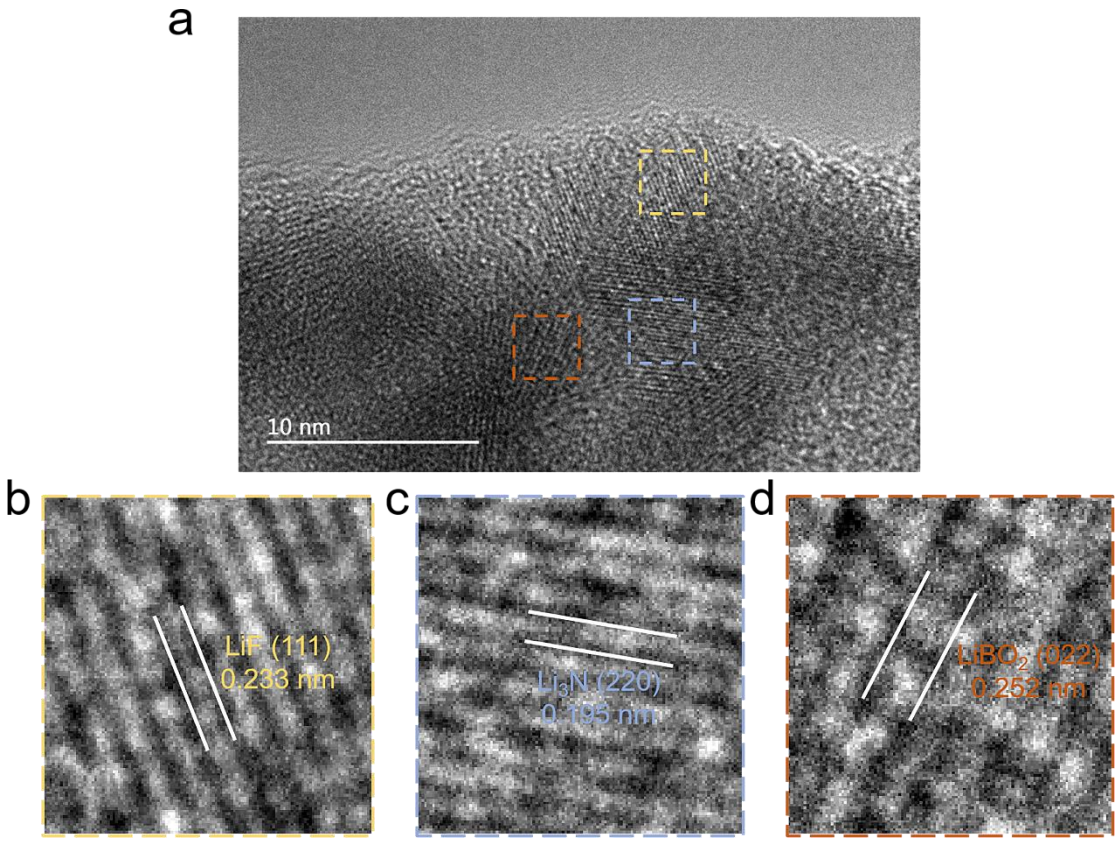

Figure S29. (a) Cryo-TEM image of the SEI formed on lithium metal using the 0.5 M-DBN electrolyte; the colored rectangles indicate the presence of LiF (yellow), Li_3N (blue), and $LiBO_2$ (maroon). The marked regions in the cryo-TEM image (a) are enlarged in (b–d), showing the corresponding nanocrystals of LiF (b), Li_3N (c), and $LiBO_2$ (d), each exhibiting distinct lattice fringes.